



UNIVERSITY OF ARKANSAS

Graduate Institute of Technology

MEASUREMENT OF THE INTENSITY OF TURBULENCE

The National Aeronautics and Space Administration
Research Grant SC-NGR-04-001-015

GPO PRICE \$ _____

CFSTI PRICE(S) \$ _____

Hard copy (HC) 3.00

Microfiche (MF) .65

FACILITY FORM 602

N67-40512

(ACCESSION NUMBER)

111
(PAGES)

CR#89614

(NASA CR OR TMX OR AD NUMBER)

(THRU)

12
(CODE)

(CATEGORY)

Status Progress Report

for

NASA Research Grant SC-NGR-04-001-015

for the Period

July 1, 1966 to June 30, 1967


MEASUREMENT OF THE INTENSITY OF TURBULENCE

Robert L. Bond

Department of Electronics and Instrumentation

University of Arkansas Graduate Institute of Technology

Little Rock



M. K. Testerman
Principal Investigator

TABLE OF CONTENTS

	PAGE
I. Introduction and Background	1
II. Work Performed	6
A. Selection of Scattering Centers (Theory)	6
1. Reflection	7
2. Rayleigh or Thompson Scattering	9
3. Mie Scattering	13
4. Miscellaneous effects	18
B. Selection of Scattering Centers (Experimental)	20
C. Experimental Setup	28
D. Experimental Studies	32
1. Alignment	32
2. Effect of Disc Velocity on Data	35
3. Location of Limiting Apertures (Effect of variation in observation angle)	37
4. Causes of Frequency Spread	40
(1) Those that were postulated but have no effect	40
a. Limiting aperture size	40
b. Particle size	42
c. Particle size distribution	42
d. Distribution caused by variations in motor velocity	42
e. Movement of the disc parallel to the incident beam	43
(2) Those that contribute significantly	43
a. Spectrum Analyzer	43
b. Convergence of the incident beam	44
c. Vertical dimension of scattering area	46
d. Horizontal dimension of scattering area	50
5. Isofrequency Lines	52
6. Frequency Measurement Limits	53
7. Noise	55
(1) Electronic noise	55
a. Photomultiplier noise	55
b. Amplifier	56
c. Spectrum analyzer	56
d. Stray electrical pickup	57
(2) Optical noise	58
a. Laser	58
b. Extraneous coherent light	58
c. Incoherent light	59
d. Misalignment or non-coincidence of heterodyned beams	60
e. Unbalance in heterodyned beam intensities	60
f. Fine lobe structure of the scattered radiation	61
8. Intensity and Signal-To-Noise Ratio	62
(1) Component reflectivity	64

(2) Lens	64
(3) Beam-splitter	64
(4) Longitudinal mode effects	66
(5) Beam spread effects	67
(6) Optical filters	67
(7) Spatial filters	68
(8) Photomultiplier	68
(9) Amplifier	70
(10) Polarization effects	70
9. Volume Scatterers	70
E. Conclusions	73
III. Future work	75
A. Polarization Effects	75
B. Volume Scattering	76
C. Fluid Flow	78
D. Readout of Data	80
References	84
Glossary	85
Appendix I	87
Appendix II	92
Illustrations	

Measurement of the Intensity of Turbulence

Robert L. Bond

I. Introduction and Background

A hydrodynamic problem has arisen in the use of high-thrust rocket engines with multiple nozzles. The flow pattern is such that the hot exhaust gases are circulated against the base of the rocket. The heating of the rocket base must be considered if a satisfactory heat balance is to be maintained. It is desirable to know the detailed flow configuration about the base of the rocket.

The determination of fluid flow patterns in the past has been limited in accuracy by the disturbances caused by the measuring probes themselves or by incomplete data in the case of optical methods. Mechanical devices are limited in frequency response. Hot wire or hot film anemometers have been used extensively in the past but the thermal time constants of these devices limit the frequency response to 200 KHz at best for a 3db down point. In addition, the probes are mechanically fragile, particularly those for high frequencies, and cannot be easily used in the determination of contaminated flow or in very-high velocity flow.

The hot wire anemometer can generally be used in pure air up to velocities of 200 m/sec without mechanical failure. In contaminated flow a coating rapidly develops which causes erroneous readings. In abrasive flow the thin film or wire rapidly erodes, producing reading errors and eventual failure of the probe. The hot film anemometer can be used in air at velocities (at atmospheric pressure) slightly above 500 m/sec and in some liquids up to 7 m/sec. The maximum temperature at which these probes can operate is approximately 150°C. The sizes of these probes are considerably larger

than the diffraction limited focus of a laser beam since the minimum length is usually between 0.5 and 1.0 mm.

The Pitot tube is limited in the determination of high-speed fluid flow since its time constant is long because of the inertia of the fluid in the readout device. It is larger than the anemometers (~ 3 mm diameter), it tends to perturb the fluid flow to a greater extent, and it is prone to errors introduced through contamination and cannot be used when solids exist in the fluid flow.

Optical systems (schlieren, interferometry, shadowgraph) used in the study of fluid dynamics are usually limited practically to laboratory situations in which their environment is closely controlled. Although these measurement techniques do not perturb the flowing system, it is extremely difficult to get quantitative information concerning the particular dynamics of a flowing system, especially for a high frequency turbulent medium. An additional problem with measurements on hot flowing systems, such as those around rocket bases and jets, is the high background optical noise generated by the gases themselves.

All of the above techniques for the study of fluid dynamics suffer from the inability to measure localized flow. Otherwise, all of the systems are flow integrators because of their large sampling volumes.

When the relative merits and disadvantages of the above techniques for fluid flow determination are considered, the conclusion is that a specialized optical system is preferable since photons will not perturb the flow and a beam of light can be focused to an extremely small spot giving a small sampling volume. This suggests using the shifted optical

Doppler signal scattered from the spot focused in the flowing system. However, until recently no technique existed for detecting this shifted signal. The spectrographs used in astronomical Doppler measurements lacked several decades having sufficient resolution. The heterodyne techniques used in microwave and radio frequency radars could not be used because of the incoherence of optical sources as well as their lack of intensity when made sufficiently monochromatic.

The advent of the continuous optical maser provided both a suitably coherent, monochromatic, and intense source as well as a detector. This combination permits evaluation of flow patterns with minimal interaction between the photon primary transducer and the flowing system.

The coherence and monochromaticity of the laser beam probe permit mixing of the Doppler frequency-shifted radiation scattered from a dynamic fluid system with a known optical frequency (local oscillator) to obtain a sufficiently low beat frequency that can be detected with optoelectronic devices.

This phenomenon is completely analogous to frequency mixing at radio-frequencies and is therefore called optical heterodyning. This modulated optical wave is transformed into an electrical signal by a high sensitivity square law detector according to

$$i = \alpha_0 + \alpha_1 E^2$$

where i is the current generated in the photodetector, E is the amplitude of the optical signal, and α_0 and α_1 are the first two constants in the Fourier expansion. Higher terms are insignificant. The output of the nonlinear optical detector may be represented on the intensity versus

frequency scale of a spectrum analyzer as a signal with a probability distribution function which should be a measure of the velocity fluctuations in a given scattering volume. Of course, more esoteric readout techniques may be necessary.

The correlation between this probability distribution function and the velocity of a flowing fluid through the Doppler equation has been established for one-dimensional laminar flow (1). In this work it was found that particle velocities could be measured by focusing a laser within a gas stream containing suspended particles. The light scattered from this focal region at a particular angle to the incident beam was recombined with a portion of the incident beam to produce the heterodyne signal. The interpretation of the heterodyne signal was contingent upon the viscous nature of the flow. In this simple case the flow was assumed to be along a single axis and the velocity vector \vec{v} reduced to a simple scalar, speed v_n , along a known axis. Since the velocity at any fixed point in the flowing system was time invariant as to direction, a single measurement of speed completely analyzed the flow pattern at the fixed point. The distribution function as seen by a spectrum analyzer would be in part caused by the distribution of velocities in the finite sampling volume. This broadened distribution function (frequency spread) and its other causes will be discussed in detail in the report. The ultimate purpose of this study is to determine the possibility of extending these measurements to the mapping of spatial velocity distribution in turbulent flow and eventually to three-dimensional turbulent flow measuring instantaneously both the direction and speed of flow at given point by making velocity

measurements along three axes simultaneously.

In particular the causes of frequency and intensity fluctuations in the distribution function, the size and effect of the scattering volume, and the scattering center properties (size, size distribution, density of distribution) as well as certain interactions must be investigated. Scattering centers will have to be bought or produced that will fulfill the theoretically or empirically determined criteria. If they are not chosen carefully, there will be severe nonlinear interactions which will invalidate the acquired data: particles that are too heavy or large will not follow the flow, particles that are packed at a high density will not scatter independently, particles that have large size distributions (polydisperse) will have a velocity distribution, particles that absorb highly will be poor scatterers, and particles that are too small will have low scattering efficiencies. In order to meet these criteria the properties of the particles must be known and these characteristics must be reproducible.

The determination of the effect and size of the scattering area and later of the scattering volume must be made. The size of this scattering center (in the broad sense) must be optimized in relation to the other parameters of the system and with respect to the degree of turbulence. The center could be so small that the only data taken is noise dealing with microscopic fluctuations. Conversely, if the center is too large, the data will be integrated over a given area and not give the true value of turbulence.

The one dimensional scattered radiation will be studied relative to data reduction, interpretation and sampling techniques, all of which

are discussed in great detail in the report. The readout of the data must also be studied in detail. The degree of contribution of the experimental setup itself to the data must be ascertained so that these undesirable effects may be eliminated, minimized, or corrected for in the readout of the data. The study will be limited to "cold" gases. A more detailed discussion of the approach to the problem as well as the results are presented in the following report.

II. Work Performed

A. Selection of Scattering Centers (Theory)

In using the scattering from a flowing system, the magnitude of the scattered radiation is extremely important. The scattering can occur at density gradients in the flowing fluid, from molecules and/or atoms and electrons of the flowing fluid itself, or the scattering may occur from natural or artificially introduced impurities in the flowing stream. Some properties of scattering will be considered before concluding which scattering medium would be most suitable for this study. The selection of a suitable scattering medium is of primary importance in the development of sufficiently intense scattering and the desired angular distribution of this scattered radiation. Polarization effects must also be included in this search for appropriate scatterers.

Scattering is usually classified into two main divisions — dependent and independent. Independent scattering occurs when the scattering of a given particle is not coupled to the scattering of any neighboring particles. This criterion is determined solely by particle separation and is met when the separation is about three times the particle radius.

Additionally, scattering may be classified as to the relationship between the frequency of incident and scattered radiation. In some cases (Raman scattering for example) there are actual quantum transitions in which there is a loss or gain in the energy and frequency of the scattered photon. This quantum effect must not be confused with the Doppler frequency shift in which energy is conserved without absorption or emission of additional quanta. This study is limited to radiation that is not fundamentally shifted upon scattering.

Scattering may also be classified according to the sizes of the particles from which the scattering occurs. In these types the frequency is not changed. There are three basic photon-matter interactions that in a broad sense may be classified under scattering:

1. Reflection $\lambda \ll d$
2. Rayleigh or Thompson Scattering $\lambda \gg d$
3. Mie Scattering $\lambda \approx d$,

where λ is the wavelength of the incident radiation in the suspending medium and d is the diameter of the scattering particles.

1. Reflection. In pure reflection the mechanical inhomogeneities are large enough that there are broad areas that appear optically flat to the incident radiation, wherein the phases of scattered light from adjacent particles will agree. The secondary waves from the atoms in the surface will cooperate to produce a reflected wave front traveling at an angle equal to the angle of incidence. Since the wavelets are additive, the scattered (reflected) wave approaches the intensity of the incident ray. Losses are primarily caused by conversion of some of the electromagnetic

vibration energy into heat (absorption) rather than re-radiating it as visible light. For monochromatic light it is relatively simple to construct surfaces that have a scattering (reflecting) extinction that is made up of less than 0.1% absorption. Therefore, this system is highly efficient. The mathematical description of such a system is simple:

$$\phi = \phi'$$

where ϕ is the angle the incident radiation makes with the normal to the scattering particle and ϕ' is the angle the scattered radiation makes with the normal. It will be noted that the scattered radiation from a perfect reflector (i.e. $d = \infty$) forms a beam that is the same diameter as the incident beam except for minimal diffraction effects caused by the laser exit aperture. That is, the scattering cross section for a beam of cross sectional area of 1.0 cm^2 approaches 1.0 cm^2 .

As d becomes of the order of magnitude of the beam diameter, the scattering is no longer ideal reflection and there is a three dimensional intensity distribution about the angle ϕ' . This radiation packet, called a lobe, becomes important in other types of scattering.

Because of the high scattering efficiency and simple theory associated with pure reflection, it would be highly desirable to utilize it in this proposed study. However, there are two major factors which prevent its use. Since the studies will ultimately be made in turbulent systems, the particles must have spherical symmetry to present the same scattering profile to the incident beam at all times since the particle orientations are time variant. However, with this shape the particle must have a high cross section to meet the criterion of flatness discussed above and as

a result a high mass and density. This high density would preclude the particle following the fluid flow accurately. If the particle were 1.0 mm in diameter it would follow the law of reflection to an extent, but even if it were a water droplet with its low density it could not follow the fluid motion into the turbulent region of flow. Highly reflective dielectrics or metals would indeed have prohibitive particle masses, the latter not following the highest viscous flow but falling to the bottom of the flow channel. Otherwise, with the best pure reflectors nothing more than integration of the turbulent flow into a generalized velocity vector along the net mass flow direction could be expected. Therefore, it is evident that reflection cannot be used.

2. Rayleigh or Thompson Scattering. Thompson scattering occurs as a result of interaction of electromagnetic radiation with free electrons. The scattering cross section is of the order of 10^{-26} cm^2 as given by

$$\frac{I}{I_0} \approx \frac{8\pi r^2}{3}.$$

Here r is the radius of scattering particles, I is the intensity of the scattered radiation and I_0 is the intensity of the incident radiation. Thompson scattering depends upon the available free electrons which in turn depend upon the degree of ionization of the atoms and molecules in the fluid. It must be noted that this makes the degree of scattering temperature sensitive because of the relationship between numbers of ions produced and the temperature of the Maxwellian gas. Therefore, because of the small scattering cross section for electrons and the statistical variations in their number, the theoretically simple Thompson scattering cannot be used.

Scattering from randomly distributed molecules and atoms has an intensity factor that is at least three orders of magnitude below that for Thompson scattering. This phenomenon, called Rayleigh scattering, can be described simply in mathematical terms. The intensity relationship is given by:

$$I/I_0 = kV^2 \lambda^{-4}$$

where V = volume of the scattering particles

λ = wavelength of the incident radiation

k = a proportionality constant

I/I_0 = the scattering cross section for random scatterers.

For random scatterers the total scattered intensity in any direction is determined by summing the intensities of all scattered waves. For ordered scatterers the amplitudes are additive. The value as a function of observation angle, θ , is

$$I(\theta) \propto \frac{1}{2} (1 + \cos^2 \theta)$$

which is symmetrical about $\theta = \pi/2$.

The scattering cross section at any observation angle becomes

$$\frac{I(\theta)}{I_0} = NV \left(\frac{2\pi n_0}{\lambda} \right)^4 \frac{a^4}{x^2} \frac{1}{2} (1 + \cos^2 \theta)$$

where $\frac{I(\theta)}{I}$ = scattering cross section for a given observation angle, θ ,

N = number of scatterers per unit volume

V = scattering volume

n_0 = refractive index of medium

λ = vacuum wavelength of incident radiation

α = polarizability tensor

x = distance from scattering center to optical receiver.

For anisotropic scatterers this equation is complicated by the necessity for taking the mean of the three principal values of the polarizability tensor as well as by a polynomial ratio containing a depolarization coefficient.

In random scatterers the total scattered intensity is directly proportional to the number of scatterers since the resultant amplitude is proportional to the square root of the number of scatterers. In particles smaller than λ the amplitude is directly proportional to the number of scatterers (proportional to mass) and therefore the intensity is proportional to the square of the number of scatterers.

The total light power scattered through 4π steradians from unit volume and unit incident intensity across a sphere of radius r is called the scattering coefficient, τ

$$\tau = \frac{4\pi}{3} \left(\frac{2\pi}{\lambda} \right)^4 N \alpha^2.$$

The relation of intensity to observation angle is simple and is symmetrical about a plane through the scatterer and perpendicular to the incident radiation. The degree of polarization can be stated in simple terms as:

$$P(\theta) = \frac{\sin^2 \theta}{1 + \cos^2 \theta}$$

where $P(\theta)$ = degree of polarization (varying from a maximum of unity at $\theta = 90^\circ$ to a minimum of zero at $\theta = 0^\circ$) and where θ = angle of observation. The desirability of using this type of scattering from a theoretical

standpoint is negated, however, by the extremely small scattering cross section of approximately 10^{-29} cm^2 .

Scattering in the case of spontaneous fluctuations of density in a homogeneous medium also comes under the Rayleigh scattering theory and therefore suffers from the same lack of intensity.

In general, the above scattering theories hold only for particles whose diameters are considerably less than the wavelength of the incident radiation. Of course, it would be desirable to use the particles (atoms, molecules, electrons or density fluctuations) of the flowing medium since they would of necessity follow the eddies of turbulent flow as well as less time variant laminar flows.

It would also be possible to utilize higher power lasers to get higher intensity scattered radiation. However, there are several disadvantages to taking this approach. First, most lasers of high intensity operate in the pulsed mode, making it impossible to have a continuous signal readout. In addition, when the radiation is focused to produce a small sampling volume, several disruptive effects occur. If the power density coupled with the electrical field strength is sufficiently high (as it almost always will be) the flowing gases will be multiply ionized with a great deal of force, causing a severe loss of optical coherence and a disruption of the turbulence pattern. Even with rather low power pulses there is a significant thermal effect between the particles of the fluid and the incident photons. Also, there can be a significant photon pressure at high intensities of radiation. In other words, with the use of high power lasers the perturbation caused by the non-linear photon-matter

interactions would be more disruptive to flow patterns than standard mechanical probes. It will be shown later that these effects are negligible for the proposed 50 mW laser.

Low power continuous CO_2 lasers could also be used since their output could be made low enough to minimize most non-linear photon-matter interactions. However, the increase in scattered intensity would be negated by the low quantum efficiencies of photodetectors at the CO_2 operating spectral line of 10.6 microns. Thermopiles would not have sufficient frequency response to be used.

There are also considerable safety hazards associated with the use of either high power pulsed lasers or the continuous CO_2 laser. The latter poses a particular safety problem because of its invisible output.

3. Mie Scattering. A segment of the particle size region ($0.1 \lambda < d < 100\mu$) (i.e. $d \approx \lambda$) between Rayleigh scattering theory and pure reflection cannot be treated by either of these simple theories. The theory in this region is extremely complex and has been given in detail only for perfectly spherical particles (2).

Mie treated scattering from spherical particles as an electromagnetic wave boundary value problem. The scattered wave amplitudes are determined as infinite series of Bessel functions of the radius multiplied by spherical harmonics in the observation angle. The scattering depends upon the ratio of the refractive index of the sphere to that of the medium in which the sphere is suspended $M = n_1/n_0$; upon the size of the sphere (radius = r); upon the wavelength of light in the medium ($\lambda' = \lambda/n_0$); and upon a coefficient

$y = 2\pi r/\lambda'$. As $\frac{n_1}{n_0} \cdot \frac{2\pi r}{\lambda'}$ approaches zero (i.e. $r \rightarrow 0$ as in Rayleigh scattering) all the terms of the series except the first vanishes, giving the classical Rayleigh equation for re-radiation from the induced electric-dipole moment in the scatterer.

As a second approximation to scattering, the induced electric-quadropole and magnetic moments are included. This approximation is good to a value of $r \approx \frac{\lambda}{6}$ and $m \approx 1.33$ (H_2O droplets in air). The degree of polarization with angle becomes a two-component series expansion even for this simple approximation.

As the particle size increases, the scattering intensity also increases, but the mathematical complexity also increases as more terms in the Bessel series become necessary to describe the scattered radiation.

In the region of the second approximation the scattering becomes asymmetric with the forward scattering lobe more intense than the back scattered lobe. In addition, the light is depolarized to an extent at $\theta = \pi/2$ for both isotropic and anisotropic scatterers.

The scattering coefficient is given by

$$\tau = N\pi r^2 f(y)$$

where $y = \frac{2\pi r}{\lambda}$ as given before. The function $f(y)$ is extremely complex but has the following limiting values

$y \ll 1$	$f(y)$ related to y^4 and λ^{-4}
$y \sim 1$	$f(y)$ related to y^2 and λ^{-2}
$y \gg 1$	approaches value of 2.

For $y \ll 1$, the function $f(y)$ is simply Rayleigh's 4-power law. As the particles become large (Mie scattering) the scattering is independent of

wavelength in the limit.

Mie theory also holds for electrically conducting particles if the complex refractive index of the conducting particle is used. Metals scatter more in the back direction than in the forward direction. Also, the value of the complex index (both coefficients) of refraction decreases with increasing wavelength such that scattering is more efficient toward the ultraviolet end of the optical spectrum.

In the Rayleigh scattering region the scattering is spherical and of small intensity. When the size of the particle becomes sufficiently large that the phase differences between light scattered by its various parts becomes significant, the amplitudes are no longer purely additive. This phase difference is maximum for back scattered light and extinction occurs at $r = \lambda/4$ and $\theta = \pi$. That is, as the particle size increases, the forward scattering increases as r^2 , while the backscattering decreases to zero at $r = \lambda/4$. As r becomes still larger, extinction occurs at $\frac{\pi}{2} < \theta < \pi$ and the lobe along $\theta = \pi$ becomes more intense. At larger values of r the intensity of the backward lobe reaches a maximum (at about $\frac{2\pi r}{\lambda} = 2.4$) and eventually moves over to $\frac{\pi}{2} < \theta < \pi$ ($\frac{2\pi r}{\lambda} > 3.0$).

During this process of increasing particle size, the total scattered intensity increases dramatically (about 10,000 as $\frac{2\pi r}{\lambda}$ changes from 0.5 to 6.0 for example). Also, the number of lobes increases from one at $\frac{2\pi r}{\lambda} = 0.5$ to several dozen as $\frac{2\pi r}{\lambda}$ approaches 10. Obviously the number and position of these lobes depend on the ratio r/λ .

If these large particles are randomly distributed, the intensities

add directly, if the criteria for independent scattering holds. The scattering intensity is greater than 10^{17} times that for Rayleigh scattering. Mie scattering depends upon the nature of the particles, their size and distribution. In general, if the particles are sufficiently larger than the wavelength of the incident radiation, the scattering is independent of wavelength. The complicating factor about Mie scattering theory is that it is a nebulous combination of diffraction and diffuse reflection theory. An additional intensity factor is gained in the larger particle scattering region where $f(y) \rightarrow 2$, since the scattering cross section is equal to twice the geometrical cross section. Half this amount corresponds to scattering through large angles and the other half corresponds to scattering through extremely small angles (3).

Mie scattering depends upon the refractive index, the electrical conducting properties, the observation angle and the shape and size of the particles, and the intensity of incident radiation. From insulating particles the scattered radiation is polarized elliptically and the major E vector of the ellipse is rotated oppositely on either side of the incident beam. The value of the polarization is generally independent of the mode of polarization of the incident beam for small angles.

Mie scattering from homogeneous, transparent, isotropic spherical particles is now discussed with particular regard to the scattered intensity as a function of the angle between the plane of polarization of the incident beam and the plane defined by the incident and scattered ray directions (called θ here), and to the degree and plane of polarization of the scattered light. A more detailed discussion can be found in the Appendix.

- (1) The plane of polarization of the light scattered from spherical, homogeneous, optically inactive particles of arbitrary size (such as water droplets) will be the same as if a portion of the incident beam had simply been reflected by a mirror placed at the particle position. Thus, in heterodyne experiments the polarization of the referenced beam and of the scattered beam will always be the same at the photomultiplier as long as the scattering particles have the properties listed above.
- (2) The intensity of scattered light will generally depend upon the angle between the plane of polarization of the incident beam and the plane defined by the incident and scattered ray directions.

A general exception to the second rule occurs if the index of refraction of the particle is sufficiently large. In this case the scattered intensity is isotropic about the incident ray direction.

Approximate exceptions also occur for particular particle sizes, which depend upon the index of refraction of the substance and the wavelength of the irradiating light. For example, water droplets of 0.2μ radius will scatter 6328 \AA light isotropically about the incident beam direction. Polystyrene spheres of 0.25μ radius will behave similarly.

A special case is that of backscattering. Since the angle θ between the incident and scattered rays is 180° for backscattering, the scattered intensity cannot be a function of ϕ . This is a perfectly general statement, and is also true of course for forward scattering ($\theta = 0^\circ$). This is covered in mathematical detail in the appendix.

Mie scattering is practically independent of the wavelength of the incident radiation, especially in the larger particle sizes. For metallic

particles the scattered radiation is dependent on the mode of polarization of the incident radiation. If the incident radiation is linearly polarized the polarization of the scattered radiation is conserved.

Therefore, Mie scattering (or more accurately, modifications of Mie scattering) is a rather undesirable but necessary compromise for the present study. Any deviation of the particles from a spherical configuration or any distribution in particle sizes complicates Mie theory to the extent that it is useless. The difficulty of theoretically analyzing this type of scattering suggests that a direct experimental attack is desirable. In fact, most of the studies of scattering from particles of Mie dimensions have resulted in tedious tabulation of the intensity and polarization functions in relation to the particle diameter-wavelength ratio, angle of observation and other pertinent parameters. Later, if it proves useful, it may be possible to develop approximate empirical equations for the specific scattering centers of interest.

4. Miscellaneous effects.

There are several phenomena that occur when photons come in contact with material particles. The effects of these phenomena in relation to these studies are now considered.

(1) Power Density. The power concentration of a 50 mW beam focused to its diffraction limit is given by

$$S = \frac{A P}{\lambda_o^2 f^2} = \frac{(0.1257 \text{ cm}^2)(50 \text{ mW})}{(0.6328 \times 10^{-4} \text{ cm})^2 (40 \text{ cm}^2)} \approx 90 \text{ W/cm}^2$$

where A = area of transmitting antenna (laser beam diameter)

P = transmitted power (output of laser)

λ_0 = vacuum wavelength of transmitted radiation

f = focal length of focusing lens

S = power density at focal point

This is sufficient power to soften low-melting-range polymers.

(2) Radiation Pressure. If a particle having a radius of 5μ undergoes collision with a beam of power density 90 W/cm^2 , the force exerted on the particle is 3×10^{-19} newtons. The equivalent acceleration of this particle is $5 \times 10^{-4} \text{ mm/sec}^2$ which is insignificant as compared to the values under consideration.

(3) Field Strength. The field strength existing at the focal point is given by

$$\begin{aligned} E &= (120\pi S)^{\frac{1}{2}} \\ &= (120\pi \cdot 90 \text{ W/cm}^2)^{\frac{1}{2}} \\ &= 184 \text{ V/cm.} \end{aligned}$$

This magnitude of field strength is not sufficient to disrupt the normal linear processes occurring at the focal point.

(4) Doppler Energy equivalence. The Doppler signal is seen as a frequency shift. At a given angle of observation this corresponds to a well defined energy increment

$$E = hf_1 - hf_2 = hf_D.$$

where E = energy equivalent

h = Planck's constant

f_D = Doppler frequency shift

At a Doppler frequency of 10 MHz the equivalent observed energy shift is

$$\begin{aligned} E &= (6.6 \times 10^{-27} \text{ erg sec}) (10 \times 10^{-6} \text{ cy/sec}) \\ &= 66 \times 10^{-33} \text{ ergs} \end{aligned}$$

which is in the range of translational energies.

B. Selection of Scattering Centers (Experimental).

As can be seen from the above theoretical discussion, the best scatterers would be flat dielectric plates of low density, and high polarizability oriented with their plane faces perpendicular to the incident radiation. These, of course, cannot be used because of their necessarily time-variant orientations in turbulent systems. The next best alternative was seen to be perfectly spherical dielectric particles with no size distribution. Therefore, much of the experimental work has been biased toward finding this type particle. However, this is not necessarily easier for experimental studies and as a result other systems were studied.

Since one of the primary goals of this study is to ascertain the variables which contribute to the characteristics of the data, it proved necessary to develop an understanding of system parameters and anomalies in a logical manner.

The particular approach which was selected was to simulate possible particle systems in a well defined two-dimensional domain. This permitted a suppression of several variables which would be present in a three-dimensional turbulent gas or liquid system. This approach permits an independent study of many of the basic parameters of the measuring system and also the induced variables.

The experimental arrangement for measuring the characteristics of the scattering centers is shown in Figure 1. The only important component

concerned with at present is the rotating disc. The amount of light scattered from this disc is measured at specific angles relative to the incident beam. Of more interest at present are the relative magnitudes of the signal-to-noise ratio as developed by the scattered light. Because of the primary purpose of obtaining scattering centers which gave lobes that were rotated at preselected angles and which were of high intensity, precise quantitative data were not taken. Despite this, considerable effort was expended toward the selection of the appropriate surface.

The study of these surfaces were based upon the necessity for knowing the following:

1. Effect of particle size on lobe shape orientation and intensity.
2. Effect of particle density on the above lobe qualities.
3. Effect of particle size distribution on the same qualities.
4. Effect of substrate condition.
5. Effect of methods of producing the particles
6. Effect of the nature of the material of which the particles were formed upon their characteristics (color, shape, electrical conductivity, etc.).

The physical properties of the different particles were determined using a shadowgraph. The opaque substrates caused the normal forward scattering lobe to be folded back along and to either side of the incident beam.

In general the following methods of application or formation of particles was used:

1. Chemical treatment of soluble substrates - Approximately thirty chemical solvents were brushed, sprayed, or poured on clean plastics such

as plexiglass or lucite. The most uniform results were obtained by pouring acrylonitrile over plexiglass. Bis (2- methoxyethyl) ether and pyridine were roughly comparable. However, several problems were associated with this technique. The particle sizes were so small that the back scattering lobes were dim and distributed over a large solid angle, the particle density was so high that the scattering was dependent, and the uniformity of particle distribution was sufficiently poor to give a constantly changing signal-to-noise ratio, which varied from practically unity to about four to one. Additional applications of acrylonitrile helped the uniformity problem, but other considerations ruled out the use of this technique.

2. Use of bulk graphite - In this case the graphite is a good absorber and the backscattered intensity is low. The graphite platelets which acted as scatterers deviated severely from the developed Mie theory but their relatively large flat areas held promise as good "reflectors".

3. Mechanical deposition of powder on substrate - Carbon deposited on a substrate was rejected because it absorbed a great deal more incident light than graphite. Zinc orthosilicate deposited easily, had particles in the desirable size region ($\sim 20 \mu$), and absorbed little incident radiation. However, since the particles were not of uniform shape, and the scattering occurred over a large solid angle, it was not possible to shape the back scattered lobes at the desired angles.

4. Paper - Several grades of paper varying from high-quality tracing paper to rough cleaning tissue supplied by MSFC were used. The highest quality tracing paper presented particles of non-uniform size, distribution and shape. The resultant scattering from the surface was exceedingly

random and the lobes could not be shaped. The scattering from the cleaning tissue was not intense enough to be seen using the only laser available for a light source. It can be speculated, however, that there is also a great deal of highly random scattering since the paper under a microscope is extremely non-uniform with scattering centers more closely approximating cylinders than spheres.

5. Glass based discs - Supramica 500, a solid mixture of mica and glass fragments, had a large amount of reflection. However, a great deal of scattering occurred below the surface causing the net scattering to be dependent. Films deposited on glass substrates and deliberately perturbed to approximate the desired particles were not successful because of the difficulty of standardizing the particle sizes, shapes, and distributions. The back scattered lobe was shaped well and was located coaxially about the incident beam.

6. Metal Surfaces - Metal surfaces were primarily prepared by sandblasting and sandpapering. The particle sizes were determined by the size of the sandblasting particles or the grit of the sandpaper. The scattering from some of these surfaces was surprisingly independent. This is probably because of the three-dimensional nature of the discs - as if the particles were suspended on a substrate whose reflected light originates from a plane sufficiently deep within the disc to not interfere with the desired scattering. This independence could be improved by applying more force to the sandblasting particles or to the sandpaper. The "smoothest" surface was prepared with crocus cloth and was completely unusable because of an almost matted finish. The roughest surface was made with "pebble"

size sandpaper and had purely diffuse scattering with low efficiency. Intermediate particles provided better scattering intensity and lobe distributions. The lobes could be shaped and rotated relatively easily by varying some of the parameters mentioned above. Of course, the ideal condition would be to have a large backscattered lobe envelope, elongated along and adjacent to the incident axis.

Obtaining uniform surfaces with either of these techniques was not difficult. In sandblasting, the distance from the point source of abrasive to the surface under preparation was the key to uniformity. In sandpapering, the biggest problem was to insure that the lines formed by the sandpaper were broken up into small segments. If this were not done, the radiation scattered from the lines produced a direction sensitive pattern. In this case a small angular segment contained the majority of the re-emitted radiation and varied its spatial position as the disc was rotated. The resultant readout consisted of good data for a small portion of a cycle and no discernable data during the remainder of the cycle. This problem was eliminated by sanding the surface in a completely random manner. The linear polarization of the incident radiation was more or less preserved in the scattered radiation so that under many conditions the heterodyned signal was reduced because of an angle between the \vec{E} vectors of the two heterodyned beams. Steel was the most efficient scatterer; aluminum was the least efficient when prepared by sandblasting. Aluminum prepared with sandpaper became the standard for future studies. The scattering centers on it had about 10 μ diameter.

Dielectric surfaces were also prepared by sandblasting. It was

not possible to use sandpaper or alumina because of the large amounts of residue remaining in the surface. Dielectric surfaces prepared by sandblasting were good analogies to a laminar fluid flow carrying suspended scattering particles since the ratio of forward to backward lobe intensities were preserved. However, it was impossible to get good quantitative data from the back scattered lobes because of the low scattering intensity using the laser available at the time these studies were made. The particle sizes, densities, shapes and distributions were suitable, Surfaces prepared with available alumina powders were unsuitable.

7. Painted Surfaces - The most effective scattering surfaces have been prepared by using a highly reflective enamel manufactured by the 3M Company. The particles of pigment in this paint more closely approximate the spherical, uniform size, dielectric spheres described by Mie theory. The lobes from this paint cannot be shaped at will but the scattered intensity is sufficiently high to recommend the use of this scattering system over any of the others. The scattering properties are not significantly changed by mechanical contact and can be used continuously at 160°F. Apparently, the absorption by the pigment approaches zero since the scattered intensity is high and practically uniform (except for the fine lobed structure inherent in scattering of coherent light) over 2π radians. According to the manufacturer it "provides directional reflectance more uniform than a freshly sanded magnesium carbonate block ..." (the optical reflectance standard).

It has been possible to separate this pigment from its binders into a dry powder. This powder has been applied to plexiglass surfaces to

provide a good analogy to a flowing stream with suspended scatterers. The forward-backward intensity ratio is consistent with that anticipated for particles of this size ($\sim 20 \mu$). In fact, the pigment appears to be promising enough to consider its use as an efficient scattering medium to be suspended in the fluid of a recirculating turbulent stream. The cost is small enough to permit its use for this purpose but the separation process is not efficient enough to permit the use of the pigment in systems that do not recirculate.

The pigment is more efficient for backscattering than other commonly mentioned scattering particles, having a "reflectance" greater than 85%. Water has a low refractive index and is transparent; therefore, it transmits a great deal of light. Spherical glass beads and plastic spheres are readily available but suffer from a high transmittance. An additional problem with any transparent particle concerns its two surfaces.

A transparent spherical particle may be considered as a short focal length lens and a highly curved mirror placed in series. Light incident upon the first surface is scattered. Then some light is transmitted to the second surface where it is again scattered. The two back scattered waves present two wavefronts to the readout device. In addition, a great deal of interference occurs between the two wave fronts. Therefore, the intensity of radiation scattered from transparent particles is reduced not only by the more efficient transmission but also by the interaction between the two surfaces of the sphere (dependent scattering). Non-spherical particles introduce more complex considerations.

Carbon particles, as mentioned before, inherently absorb light and

are not nearly so efficient as scatterers as the pigment is.

At the same time, studies were attempted on volume scatterers. These studies were not successful for two reasons. The scatterers that were available were polymers and did not give independent scattering. Bulk Teflon (which is thought to be a combination of amorphous and crystalline material) and polyethylene were used. Their dependent scattering was immediately obvious since the entire disc became a secondary emitter of the incident radiation. In addition, at the time these studies were made there was not sufficient incident intensity to discard a large amount of light at the surface of a volume scatterer and still have enough intensity left at the scattering volume.

All of the dielectric particles mentioned above scatter any incident radiation as elliptically polarized light. The metals preserve the polarization condition of the incident light. As yet no thorough experimental study of the polarization character of the scattered light has been made. Only sufficient information to test the general behavior of the scattering of the incident linearly polarized light was made for the purpose of attempted optimization of the heterodyne signal.

Each of the small lobes making up a large lobe consists of slightly different degrees of elliptical polarization. Therefore, the size of the readout apertures are important in optimum matching of polarization vectors. However, the size of the aperture is more important in its own right above certain small diameters since doubling the area of the aperture doubles the signal whereas it is only possible to approach doubling the signal by matching polarization vectors.

C. Experimental Setup.

Figure 1 shows the general form of the apparatus that was used to study the discs discussed above and, with small changes, all of the data taken until now. Figure 9 shows the current setup as it has evolved from the initial device.

Since the configuration used differs considerably from previously used arrangements, it will be worthwhile to discuss reasons for its selection. The backscattered configuration was initially chosen because of the desirability, and indeed the necessity, of using it in a determination of the flow about the base of a rocket. The symmetric, dual scattered beam heterodyne configuration was chosen because of the inherent ability of the arrangement to cancel the frequency spread because of the finite width of the limiting apertures and to compensate for changes in modulation index caused by time variant scattering intensity. By using the symmetric configuration the effective frequency is doubled, and the spread in this frequency is that caused by an aperture of zero diameter. If a single scattered beam were beat with the unshifted incident beam the frequency spread would be a linear function (at small observation angles) of the aperture diameter. This measurement was made by scanning a slit across the beams perpendicular to their axes. This can be seen by considering the equation relating the frequency of the Doppler shift to the angle of incident radiation relative to the velocity vector and the observation angle relative to the incident beam:

$$f_D = \frac{2 V_n}{\lambda_0} \sin \frac{\theta}{2} \sin \left(\psi + \frac{\theta}{2} \right)$$

where

v_n = velocity along a given coordinate system at the focal point

λ_o = vacuum wavelength of the incident radiation (6328Å for a He-Ne laser)

θ = Observation angle relative to incident radiation

ψ = Angle between the velocity component and the incident radiation

f_D = Magnitude of the Doppler frequency shift.

For a system in which $\psi = \frac{\pi}{2}$ and the incident radiation can be approximated as having no beam size or convergence angle, the equation becomes simply

$$f_D = \frac{v_n}{\lambda_o} \sin \theta.$$

For benefit of calculating the center frequency at which the Doppler shifts occurs, this approximation becomes exact.

The use of optical filters to attenuate the primary beam to an intensity equivalent to the scattered beam (this is done to eliminate the large optical D.C. bias) introduces interference fringes which cause an increase in noise and a resultant decrease in signal-to-noise ratio. For a symmetric sampling arrangement, the total Doppler shift is simply twice that given by the above equation; i.e.

$$f_D (\text{Tot}) = 2f_D.$$

It will be necessary to modify this equation for studies of turbulent flow. In this case v_n becomes a 3-vector and θ and ψ will probably be written as distribution functions in the general consideration.

The initial reason for choosing the symmetric configuration was to take advantage of the factor of two increase in frequency. This immediately

permits ignoring some perturbations that occur at low frequencies - laser mode noise, mechanical vibrations, relatively low frequency electrical pickup, etc. In addition, within a given spectrum analyzer dispersion, a higher center frequency permits a lower error relative to the center frequency since the error caused by the uncertainty of readout is constant with dispersion.

Additional problems occur when a scattered beam is heterodyned with a beam taken from the incident beam or from the rear of the laser as was done in several experiments. The non-scattered beam is inherently more intense than the scattered beam. In the process of attenuating the beam to be more nearly equal to that of the scattered beam, interference fringes are introduced which lower the overall intensity (heterodyne current). In addition, the system becomes more vibration sensitive because of the movement of the interference fringes.

The plane polarized light from a Perkin Elmer 5200 laser with an output of 0.5 mW impinges, after passing through several spatial filters, upon a 5 inch lens (not highly corrected, see Figure 2) which focuses the beam upon a rotating disc. The focal length of the lens is approximately 8 inches. The rotating disc is mounted on a high speed D.C. aircraft pump motor which is powered by a series of wet cell D.C. batteries. The incident beam is focused on the vertical axis of the disc and approximately 1.0 inch above the horizontal axis. The vertical axis is chosen to give symmetry of the isofrequency lines about the incident beam. The distance from the horizontal axis is not critical and is variable. However, as will be seen later, the frequency spread decreases as this distance increases. Variation of this distance affects the frequency of the scattered radiation

in a linear manner.

Determination of the exact location of the focal point is extremely difficult. The best procedure found to date is dependent upon the aberrations introduced into the back scattered beam by the lens. However, it is used in lieu of any more precise method. First, the limiting apertures and beam splitter are removed and the scattered light through one half of the lens is allowed to impinge upon a mirror, which may be the mirror typically located in the system, which reflects the beam over a distance of about fifteen feet. A large aperture, or a matrix of small apertures, is placed in the beam near the mirror. At the terminus of the beam a replica of the aperture or matrix is placed in the beam. The lens position is then varied along the optical axis until the beams defined by the first aperture or matrix coincide with the duplicate at the other end of the beam. A large aperture or several small ones are chosen to minimize the uncertainty caused by diffraction at the edges of all apertures. A distance longer than fifteen feet would be preferable except for the barrel distortion of the lens. The location of the focal point can be roughly determined by filtering out the scattered coherent light to the eye and minimizing the size of the focused incoherent light.

It is also important that the disc be perpendicular to the optical axis in order to maintain the symmetry of the device. Otherwise the value of ψ is different on either side of the incident beam.

The radiation is scattered from a point on the disc according to the conditions of the particles on the disc as discussed above. All of the rays that are backscattered through the lens are made parallel

again (within limits of the correction of the lens). Two segments on the horizontal axis and spaced symmetrically about the incident beam are intercepted by circular apertures forming pencil beams. The distance from the apertures to the incident beam were variable in earlier experiments. Variation of these distances change the observation angle, θ , which results in a change in the value of the frequency of scattered radiation.

The two cylindrical beams are intercepted by a mirror and a beam splitter respectively and brought together on the face of a DuMont 6911 photomultiplier whose output is read on the cathode ray tube of a Singer Panoramic SPA-3/25a spectrum analyzer.

D. Experimental Studies.

Utilizing this basic setup, some of the experiments carried out and some problems that have arisen can be discussed. The primary experimental goal has been to determine what parameters contribute to the overall characteristics of the data and to build a solid basis for studies of turbulent flow.

1. Alignment. One of the most difficult early problems was the alignment of the beams to an accuracy sufficient to get a workable signal-to-noise ratio. Part of the problem was an unbelievably naive idea of the criteria necessary to produce maximum heterodyne current at the output of the photomultiplier. Through a tedious manipulation of variables, an overall view of the necessary criteria began to unfold. Later, after an unpublished report by Lee (5) was made available, the close approximation between the experimentally determined criteria and those predicted by Lee was encouraging. The factors which were found to affect the quantity of heterodyne current were:

1. Angular separation between two parallel beams.
2. Spatial separation between two parallel beams which are also mutually parallel.
3. Misalignment of the major axes of the of the polarization ellipses of the scattering radiations.
4. Deviation of one or both of the heterodyning beams from parallel.

An additional consideration predicted by Lee that has not been seen experimentally in this apparatus concerns the size of the photomultiplier aperture, which in this case is determined by the 0.154 inch diameter of each of the defining apertures in the backscattered beam. In the process of another experiment, apertures larger than one inch in diameter were used with no apparent reduction in the extrapolated heterodyne current because of loss of spatial coherence at the large aperture.

It experimentally was determined that a distance of at least 15 to 20 feet was necessary as a lever arm to suitably align the two beams. That is, if within the ability of the eye to resolve, the beams are made coterminous over a distance of greater than fifteen feet, the heterodyned current is optimized as to angular and spatial separation. Theoretically, the larger the lever arm the more accurate is the alignment and the higher the heterodyne current. However, because of a barrel distortion in the lens, any larger distance of alignment introduces an uncertainty which usually leads to reduced heterodyne current.

Of special importance in the alignment procedure is that the two beams coincide at the beam splitter both vertically and horizontally. This criterion is frequently hard to meet because of obvious observation

problems. There are two procedures that are mutually complementary in determining whether the beams are sufficiently coaxial. First, with the disc stationary the two beams are "walked" as nearly as possible into coincidence. In this case the natural room vibrations become extremely important. If the two beams are completely coincident there will be a low frequency flicker of the net beam intensity as the phase differences of the two beams alternately attempt to cancel and complement the beam intensities. This case is analogous to the case of two coincident non-scattered beams which can be made to completely cancel (180° out of phase) or complement each other - in the first case effectively cutting off the laser, in the second case doubling the amplitude of the beam. As the beams deviate from coincidence, the interference is an angular effect causing the transition from no fringes (at coincidence) to large numbers at relatively small angles of separation. Since interference no longer is angle independent, it is not complete over a long linear segment of the beams. Therefore, the positioning of the photomultiplier becomes critical and the system is vibration sensitive. An alternative was to look at the low frequency Doppler signal on an oscilloscope, and adjust it to maximum. This was impractical with the spectrum analyzer. Obviously it is desirable to have the light spread over as much of the interfering beams as possible. A technique that was felt would help compensate for misalignment was to focus the beams onto the surface of the photocathode. This would effectively make all rays parallel at the focal point. This technique was soon discontinued because of the difficulty of obtaining the true focal point, because of the sensitivity to vibration as the photocathode oscillated about the

focal point, and because of a reduction in heterodyne current due to losses at the lens. Later, the basic concept of focusing the heterodyned beams was found to have been predicted by Lee. In theory the concept is good; in practice it would be so difficult to implement that it is not worth the effort, as was experimentally determined.

The second check on the beam alignment (which incidentally checks the difference in parallelism of rays within the two beams) is performed with the disc rotating. The rotating disc integrates the mottled appearance of each of the two beams into two uniform light discs with well-defined edges. Over the distance of fifteen feet the edges of the beams can be made coincident to a high degree of accuracy. It was not possible to use an oscilloscope to align this high frequency Doppler. The peak could be maximized using a spectrum analyzer, but this technique was very difficult.

Experimental evidence indicates that by properly utilizing these suggested alignment techniques, the heterodyne current is nearly maximum and any other additional attempts are extraneous.

It is also important to have the components affecting the incident beam coaxial about it. If not, the spatial filters will remove important radiation. If the lens is not centered on the incident beam, the resultant scattering is skewed. The criteria may be met by reflecting the light until it re-enters the laser.

2. Effect of Disc Velocity on Data.

The use of a variable velocity medium was initially used to permit simulation of the different velocities that had been used by Brown in their "laminar" flow measurements. For a reasonably compact system with

disc radius $R = 2.5$ inches this would require a motor speed of 0.75 rpm to 43,545 rpm, corresponding to gas velocities from 0.5 to 28,956 cm/sec.

In a 0.5 cm diameter tube, turbulence occurs for air according to $v =$

$$(Rn) / D\rho = 362 \text{ cm/sec}$$

where $\rho = 1.213 \times 10^{-3} \text{ gm/cm}^3 = \text{density of air}$

$\eta = 1.827 \times 10^{-4} \text{ gm/sec cm} = \text{viscosity}$

$D = 0.5 \text{ cm}$ (tube diameter)

$R = 1200 = \text{Reynolds number for turbulent flow.}$

The D.C. motor mentioned above has a capability of about 100 rpm to greater than 13,500 rpm with a great deal of velocity variation — as much as 10% at midrange, more at low velocities. Because of severe vibrational problems at higher speeds, the practical use was limited to rather short periods because of component misalignment. This motor, powered by D.C. batteries, was sufficient for the intensity measurements described above. However, later measurements depended on a more stable center frequency for the measurement of this center frequency as well as the width of the display (frequency spread) on the spectrum analyzer. An attempt was made to use a unijunction-SCR D.C. motor regulator designed by General Electric. This regulator was supposed to be continuously variable in output voltage and as a result would give the motor a highly regulated continuously variable frequency. It turned out to be neither continuous nor a regulator at most frequencies.

In the earlier studies without the regulator and at the incremental frequencies at which the regulator would work, it was noted that the velocity of the motor had no measurable effect (other than the linear

effect postulated by the Doppler equation) on the frequency spread or on the center frequency. Of course, at velocities at which mechanical vibrations become large, there is an effect probably caused by the misalignment of the system.

As a result of the above conclusion it was decided to use a synchronous motor driven by a variable (280-520 cps) frequency generator which has a frequency accuracy of 0.5% and a temperature coefficient of $\pm 0.01\%/^{\circ}\text{C}$. This permitted a motor speed of about 8380-15,570 rpm which, on the basis of the independence of velocity and frequency nonlinearities, is completely acceptable. Any shift in center frequency is too small to be measured or seen.

All of the measured values of frequency shift agreed with those predicted by the Doppler equation which was also checked. This, of course, was not true until the uncertainties were removed. This depends upon accurate measurement of θ , ψ , and the velocity of the disc.

3. Location of Limiting Apertures (effect of variation in observation angle). It has been noted before that the limiting apertures are located symmetrically on the horizontal axis and on either side of the incident beam. Since the focal length of the lens is fixed, the position of the apertures uniquely determines the magnitude of the observation angle. In the early experiments the lens had a focal length of ~ 8.0 inches and the apertures were spaced to give an observation angle of 6.0° on either side of the incident beam. At an equivalent velocity of 880 cm/sec (2800 rpm with $R = 3$ cm) this gave a total Doppler shift of

$$f_D = 1.45 \text{ MHz}$$

and

$$2f_D = 2.9 \text{ MHz.}$$

Of course, this value is linearly related to higher or lower values of frequency as long as θ remains small. For example, the deviation of $\sin \theta$ from θ at 15° is only 1.15%. This error becomes 0.13% at 5° .

Under conditions of small θ and $\psi \approx 90^\circ$ the following approximations may be made

$$\sin(\psi + \frac{\theta}{2}) \approx 1$$

$$\sin \frac{\theta}{2} = \frac{\theta}{2}.$$

Now, the Doppler equation reduces to

$$f_D \approx \frac{v\theta}{\lambda_0}$$

such that the value of f_D is effectively a linear function of the observation angle.

The variations of f_D from a linear function within the limiting angles defined by the lens aperture are shown in Table 1.

TABLE 1

Observation Angle (θ)	f_D exact (MHz)	f_D Approx. (MHz)	% Error	$2 f_D$ (exact) (MHz)
$17^\circ 20'$	13.6777	13.8884	1.54	27.36
15°	11.8822	12.0190	1.15	23.76
10°	7.9721	8.0125	0.51	15.94
$6^\circ 32'$	5.2235	5.2350	0.22	10.46
6°	4.7989	4.8076	0.18	9.60
$5^\circ 31'$	4.4137	4.4201	0.15	8.83
5°	4.0014	4.0065	0.13	8.00

These values were calculated at a velocity of 2,905 cm/sec, which is an acceptable value for turbulence and was obtained easily with a rotating disc. The maximum half-angle subtended by the 5 inch lens is $17^{\circ} 20'$. Therefore, the maximum possible error using the edge of the lens as a limit is 1.54%. That is, for practical considerations the position of the apertures has no significant effect on the linearity of f_D . Here, for a symmetric system the readout frequency is $2f_D$.

The angle $6^{\circ} 32'$ defines the limiting angle of the framework of the corrected 4 inch lens. As an indication of the total accuracy of the system in relation to calculated and measured values of $2f_D$ consider the $6^{\circ} 32'$ angle and the $5^{\circ} 31'$ angles, representing the range of errors. In the first case the measured value of $2f_D$ was 10.4593 MHz, the calculated value was 10.4471 MHz giving an error of 0.117%. In the second case the measured value of $2f_D$ was 8.8599 MHz, the calculated value was 8.8274 giving an error of 0.368%. Both of these values are well within experimental error. If the two apertures are not equally spaced, however, error is introduced from several sources. First, the system is no longer symmetric, introducing a spread in frequency because of the non-superposition of the correct rays coming through the apertures. In addition, there is a shift in the center frequency for the same reason. This also invalidates the simple process of assuming that $f_D (\text{tot}) = 2f_D$, therefore complicating calculations.

The experimental determination agrees completely with the calculated values. The equality of the angles was checked by beating each backscattered

beam with an unshifted beam. The center frequency of the two beams agreed, indicating that both sampling angles are equal.

4. Causes of Frequency Spread.

The peak, as displayed on the spectrum analyzer, has a finite width. Since it is proposed to use the probability distribution function on the spectrum analyzer to study the turbulent flow of a fluid process, it is necessary to fully understand the causes of the frequency spread and eliminate these causes if possible. This understanding is crucial to the use of the heterodyne technique for determination of the characteristics of turbulent flow. If it is not possible to eliminate the causes they must be considered quantitatively in the data.

This degree of contribution of external effects and system parameters to the width of the frequency spectrum must be known because of the time variant characteristics of turbulent flow. In other words, the time variant nature of turbulent flow produces a frequency spread of its own. It is postulated that the characteristics of this spread will be used to determine the characteristics of turbulent flow. If external effects also exist producing a distribution of their own, the desired distribution will be masked out or its characteristics will be modified.

The classification of the possible causes of frequency spread fall in two classes: (1) those that were postulated but do not contribute to the spread, and (2) those that contribute significantly to the spread.

(1) a. Limiting Aperture Size.

In systems utilizing heterodyning between an unshifted beam and a shifted beam, the spread in Doppler is a sine function of the aperture size as given by

$$\Delta f_D = \frac{2V}{\lambda_0} \left[\sin \frac{\theta_1}{2} \sin \left(\psi + \frac{\theta_1}{2} \right) - \sin \frac{\theta_2}{2} \sin \left(\psi + \frac{\theta_2}{2} \right) \right]$$

$$= \frac{V}{\lambda_0} \left[\sin \theta_1 - \sin \theta_2 \right] \text{ if } \psi = \frac{\pi}{2}.$$

If θ_1 and θ_2 are small the relationship becomes linear

$$\Delta f_D = \frac{V}{\lambda_0} \left[\theta_1 - \theta_2 \right].$$

Here Δf_D is the spread in frequencies and θ_1 and θ_2 are the observation angles defined by the inner and outer edges of the limiting apertures respectively. This was checked experimentally by scanning a slit across the mixed beam resulting from combining a scattered beam with a direct beam of about the same size and intensity. The resultant plot of frequency versus distance is effectively the integral of a Gaussian curve.

On the other hand, when the mixed beams were both scattered in the perfect symmetric manner described above and shown in more detail in Figure 3, the resultant frequency spread was zero. Since only the difference frequency is seen by the photomultiplier, the frequency distribution at the apertures is that given in Table 2.

TABLE 2

Aperture	Center	Top Edge	Bottom Edge
#1	$f + 2\delta f$	$f + 3\delta f$	$f + \delta f$
#2	$f - 2\delta f$	$f - \delta f$	$f - 3\delta f$
#3	f	f	f

It can clearly be seen that the top beam is inverted such that the following differences hold:

$$f_C = (f + 2\delta f) - (f - 2\delta f) = 4\delta f$$

$$f_T = (f + 3\delta f) - (f - \delta f) = 4\delta f$$

$$f_B = (f + \delta f) - (f - 3\delta f) = 4\delta f$$

which is exactly twice the Doppler shift at the center of either aperture.

Therefore,

$$\Delta f = f_C - f_T = f_T - f_B = \dots = 0$$

and there is no frequency spread. This can be checked easily by using larger apertures or by scanning a slit across the beam. Both techniques gave the same result: $\Delta f = 0$. For this to be true the two apertures must be accurately spaced and the two beams must be coterminous.

b. Particle Size. There is no net frequency spread since the Doppler frequency is a function of velocity of the particles and in the Mie scattering range particles are small enough to have practically no velocity spread (that is, they follow the flowing stream linearly). This holds for particles fixed in a matrix and in a flowing gas stream.

c. Particle Size Distribution. If the distribution of particle sizes is small (since Mie sized particles are being considered) the resultant velocity distributions are small because approximately the same force is acting on all particles and the resultant spread in Doppler frequencies is small except at very low velocities where the distribution of velocities becomes significant in relation to the mean velocity (translational motion of the molecules). This latter value is insignificant for this high velocity study.

d. Distribution Caused by Variations in Motor Velocity. Formerly this gave a significant spread as the center frequency varied up and down the frequency scale. Currently the motor speed is so constant that a variation cannot be measured with available equipment. Therefore, this contribution becomes negligible.

e. Movement of the Disc Parallel to the Incident Radiation (caused by bent shaft, disc of nonuniform thickness, deviation of disc from perpendicularity to beam, or warped disc). This would effectively change the size of the beam continuously during a rotation and would result in changing scattered intensity and in a spread because of the beam size (see section below). The contribution to frequency spread due to these causes can easily be minimized and as a result is not considered.

(2) The following factors contribute significantly to the frequency spread as seen on the spectrum analyzer.

a. Spectrum Analyzer. A spectrum analyzer has a certain inherent peak width in its display of a function. If a line frequency of ± 0.0 is displayed on the spectrum analyzer it will be read as $f \pm \frac{\Delta f}{2}$, where Δf is the total frequency spread. This spread is a function of the video filtering, the sweep rate and the sweep width, but is primarily a function of the IF bandwidth of a spectrum analyzer. Because of its dependence on the IF bandwidth, it is of primary importance to have a maximum signal-to-noise ratio. This difficult problem will be discussed in more detail later.

Before any meaningful studies could be made on the width of the frequency spread caused by the remainder of the system, it was necessary to substitute a Spectra Physics 125 laser with an output of greater than 50 mW for the 0.8 mW laser so that the signal-to-noise ratio could be increased. This change permitted measurement of the frequency spread caused by other effects. The inoperative spectrum analyzer borrowed from MSFC has a low frequency spread limit and can potentially be used

in a certain frequency region to study the other effects discussed below. Ironically, its sweep width may be so narrow that the other effects will prevent the use of the 1L10.

The width of the Doppler signal using the 0.8 mW laser was approximately 65 KHz with a signal-to-noise ratio of 4-to-1, if one back scattered beam was heterodyned with an unshifted beam. If both backscattered beams were heterodyned, the width was limited by the 50 KHz of the Singer spectrum analyzer.

The salient characteristics of the three spectrum analyzers which are used are:

TABLE 3

Spectrum Analyzer	Resolution (IF Bandwidth)	Dispersion (Sweepwidth)	Sweep rate
Singer SPA-3/2Aa	200Hz - 25KHz	300Hz/cm - 300KHz/cm	0.1 sec/cm - > 1msec/cm
Tektronix 1L10	10Hz - 1KHz	10Hz/cm - 2KHz/cm	< 1sec/cm - > 5msec/cm
Tektronix 1L20	1KHz - 100KHz	1KHz/cm - 10MHz/cm	< 1sec/cm - > 5msec/cm

As noted before, the values are inter-related and therefore the value of one depends upon setting of others. These values were measured at half peak height. Generally the value is multiplied by 2.0 at 5% of total peak height.

The sweep rate is a major problem with the Tektronix spectrum analyzers. At low sweep rates the resolution is maintained but phosphorescence of the CRT screen is too short to study well; at higher sweep rates where the CRT display is acceptable the resolution and, therefore, peak amplitude deteriorate .

b. Convergence of the Incident Beam. Consider Figure 4 which is a distorted representation of the focused beam converging onto the scattering plane

moving with velocity, \vec{v} . The size of the beam entering the front surface of the lens is 2 mm in diameter to the 1/e power points. The focal length of the lens is 400 mm. Assume for now that all rays from the incident beam coincide at a single point in the scattering plane. The half angle is defined as $\phi/2 = \tan^{-1} \frac{1}{400} \approx 10$ minutes of arc. This indicates the presence of two extreme conditions defining a maximum and minimum Doppler shift. Consider the observation angle, θ , to be defined as the angle between the center of one limiting aperture and one of two rays defining the convergence angle of the incident beam. The value of ψ is defined as the angle between \vec{v} and one of the two rays defining the convergence angle. Under ideal assumptions ($\phi = 0$), $\psi = 90^\circ$, and $\theta = 6^\circ$.

However, if $\phi \neq 0$ the values of ψ and θ deviate, introducing different Doppler frequency values. The important values are in Table 4 where $v_n = 632.8$ cm/sec.

TABLE 4

Limit	θ	ψ	f_D (MHz)
min	$5^\circ 50'$	$89^\circ 50'$	1.016
max	$6^\circ 10'$	$90^\circ 10'$	1.074

The frequency difference

$$\Delta f_D = \frac{2v_n}{\lambda_o} \left[\sin \frac{\theta_{\max}}{2} \sin \left(\psi_{\max} + \frac{\theta_{\max}}{2} \right) - \sin \frac{\theta_{\min}}{2} \sin \left(\psi_{\min} - \frac{\theta_{\min}}{2} \right) \right]$$

$$= f_D (\max) - f_D (\min) = 57.6 \text{ KHz}$$

which is the spread of frequencies introduced into the signal by the convergency angle and is 5.51% of the center frequency and is a linear function of velocity. These values were calculated from the standard Doppler equation. Since the optical system is symmetrical, the values

are the same for the other aperture. The Doppler frequency spread is not canceled out in this case, however, because of the random manner in which the frequency shifts are distributed at the limiting apertures. The entire Doppler equation must be used here since $\psi \neq \pi/2$.

It was not possible to measure this Doppler frequency spread directly because of the contribution of other factors. Instead an indirect measurement was made using an optical collimator to increase the diameter of the beam from 2 mm (Gaussian 1/e power points) to a 50 mm (rectangular intensity cross section) incident beam.

Making the same calculations as before,

$$\frac{\phi}{2} \approx 3^{\circ}30'$$

and Table 5 gives the parametric values.

TABLE 5

limits	θ	ψ	f_D (MHz)
min	$2^{\circ}30'$	$86^{\circ}30'$	0.436 MHz
max	$9^{\circ}30'$	$93^{\circ}30'$	1.639 MHz

This gives a Δf_D of 1.2 MHz for a calculated value. The approximate measured width was 1.0 MHz. This was low for three reasons: uncertainty in measurement of width because of flattened display, decrease in vertical spot size, and decrease in horizontal spot size because of diffraction limit decrease. This clearly indicates the deleterious effects large beam convergence can have.

This leads also to the next cause of Doppler frequency spread since the beam convergence is inversely related to diffraction limit at small angles.

c. Vertical Dimension of Scattering Area. The size of both the vertical

and horizontal dimensions of the focused spot are practically limited by the diffraction laws. Therefore, the theoretical spot size which corresponds to an aplanatic lens or one with f/number of unity cannot be obtained without sacrificing other desirable characteristics. The aperture of an optical system through which a laser beam passes is defined by the diameter of the laser beam and not by the lens diameter. Therefore, the f/4 lens of this optical system becomes effectively a f/200 lens because of the 2 mm diameter of the laser beam. Conversely, if a lens were chosen to give f/1 so that the theoretical focus is obtained, the focal length would be 2 mm, making a serious engineering problem. In addition, the incident convergence angle increases from ~ 20 minutes of arc to greater than 53 degrees, which distributes the frequency spread over an effectively infinite range.

The absolute minimum spot size for a Gaussian beam with aperture f/1 and plane polarization is given as an ellipse with major axis $1.5 \lambda / \pi$ and minor axis λ / π . This corresponds to the 1/e power points which comprise 63.2% of the beam power. The ellipsoidal shape is caused by the oscillating dipoles which radiate more strongly along one axis than the other. (7)

As the f/number increases from the aplanatic lens case the significance of the theoretical limit becomes less important. The value of the diffraction limited focus would generally be the absolute spot size times a ratio which considers the f/number. The equations for this case then become

$$\frac{1.5\lambda}{\pi} \cdot \frac{f}{d} \text{ and } \frac{\lambda}{\pi} \cdot \frac{f}{d}$$

This increases the minimum beam size by a factor of 200, the f/number defined above.

For $\lambda = 6328\text{\AA}$ the ellipsoidal dimensions are approximately 60μ by 40μ . The corresponding null-to-null diameter (Airy disc, containing 81% of power) of the usual circular diffraction pattern using unpolarized light is given by

$$\frac{3.83\lambda}{\pi} \cdot \frac{L}{d} = 153\mu.$$

This is a more realistic value to be considered for the actual case because scattering prior to reaching the focal point, divergence of the laser beam, and the entire beam (as opposed to the 1/e power point) as well as other anomalies must be considered. The figure agrees roughly with that obtained from actual measurements. The value obtained by measurement was taken at other than the 1/e power point and extrapolated along the normal distribution curve to be about 261μ . The corresponding Airy disc diameter was 276.6μ . Direct measurement was not possible because of the unavailability of appropriate apertures.

This value for the Airy disc will be used in the following calculations as a form of worst case analysis. The vertical dimension of the focused spot contributes to the Doppler frequency spread because of the possibility that it will contain several velocities. This is analogous to the scattering volume problem. The two dimensional case is simple and demonstrates what effect velocity distribution plays in signal spread.

Consider a perfectly parallel incident beam of diameter $d = 276.6\mu$ corresponding to the focal spot size discussed above (Figure 5). In this case, the light scattered from the top of the spot (where the disc

velocity is higher) will be at a higher frequency than the light scattered from the bottom portion of the spot. Since the angles θ and ψ can be assumed to be unaffected without loss of generality, the simple form of the Doppler equation can be used:

$$f_D = \frac{v_n}{\lambda_o} \sin \theta.$$

Now

$$\Delta f_D = f_D (\max) - f_D (\min) = \frac{\sin \theta}{\lambda_o} (v_{\max} - v_{\min}).$$

But by writing v_n in terms of the disc radii under consideration, the equation becomes

$$\Delta f_D = \frac{v_n}{R\lambda_o} \sin \theta (R_{\max} - R_{\min}) = \frac{v}{R\lambda_o} \sin \theta \Delta R$$

where Δf_D = frequency spread

v_n = mean linear velocity of the disc = 632.8 cm/sec

R = mean radius of the disc = 2.324 cm

ΔR = spot size = $276.6\mu = 0.02766$ cm.

The quantity Δf_D can be calculated to be

$$\Delta f_D = \frac{(632.8)}{(0.915)(2.54)(6.328 \times 10^{-5})} (\sin 6^\circ)(0.02766)$$

$$\Delta f_D = \frac{(632.8)(0.10453)(0.02766)}{(0.915)(2.54)(6.328 \times 10^{-5})}$$

$$\Delta f_D = 12.42 \text{ KHz}$$

The values of v , R , λ_o , and θ will be constant for a given system and the frequency spread can be directly related to the spot size by considering the following

$$f_D = \frac{v_n}{\lambda_o} \sin \theta = \left(\frac{2\pi f}{60\lambda_o} \right) R \sin \theta$$

$$\Delta f_D = \frac{2\pi f}{60\lambda_o} \sin \theta \Delta R.$$

By dividing the first equation by the second a direct ratio is set up:

$$\frac{f_D}{\Delta f_D} = \frac{R}{\Delta R},$$

which indicates that the frequency spread is a direct function of the vertical spot size. In the above equation f is the motor speed in revolutions per minute. A calculation of Δf_D using this equation agrees with the above calculated value

$$\Delta f_D = \frac{f_D}{(R/\Delta R)} = \frac{1.045 \text{ MHz}}{(2.54 \times 0.915)/(0.02766)}$$

$$\Delta f_D = 12.43 \text{ KHz.}$$

d. Horizontal Dimension of Scattering Area. The other orthogonal dimension of the focused spot contributes nothing to the frequency spread as far as direct velocity variations are concerned. However, the effective observation angle is changed by the finite horizontal dimension of the spot, as shown in Figure 6. Of course, the leading and lagging edges of the focused spot are not at exactly the same radius as the center of the spot but, because of the small spot dimension, the value of ΔR is small enough to be negligible in the considerations in this case. Because the effect discussed here is simply a function of spot size the simple equation can again be used as a basis

$$f_D = \frac{v}{\lambda_0} \sin \theta$$

which becomes

$$f_D = \frac{v}{\lambda_0} (\sin \theta_1 - \sin \theta_2)$$

where θ_1 defines the angle between the normal and the lagging edge of the spot and θ_2 defines the angle between the normal and the leading edge of the spot. By construction of the parallel line h_2 , it can be seen that

the contribution of horizontal spot size is the same as for aperture contribution when a single scattered beam is mixed with an unscattered beam.

In terms of the geometry of the system this equation becomes

$$\Delta f_D = \frac{v_n}{\lambda_o} \Delta (\sin \theta) = \frac{v}{\lambda_o} \left[\frac{a}{\sqrt{f^2 + a^2}} - \frac{a - x}{\sqrt{f^2 + (a-x)^2}} \right]$$

where a = the distance from the optical axis to the outer terminus of
a limiting aperture

x = horizontal spot size

f = lens focal length = 40 cm.

This value of frequency spread, which for a symmetric system is the same at the external edge of each limiting aperture, is random and is not cancelled out by the beam overlapping. Since the value of $\theta \approx \sin \theta$ for small values of θ , the value of Δf_D is practically constant over rather large values of θ . For example, with a change in the quantity a of a factor of two there is no change in $\Delta \theta$ until the third decimal place. Here the value of f_D is, of course, a linear function of angular spread (spot size).

Upon calculation, the value of f_D becomes

$$\Delta f_D = \frac{v_n}{\lambda_o} \left[\frac{(1.881)(2.54)}{\sqrt{(40)^2 + [(1.881)(2.54)]^2}} - \frac{(1.881)(2.54) - 0.02766}{\sqrt{(40)^2 + [(1.881)(2.54) - 0.02766]^2}} \right]$$

$$\Delta f_D = 6.8 \text{ KHz}$$

The values of these parameters which cause frequency spread have been shifted around (some increased, others decreased) to give a more nearly optimized value. The total width has decreased as a result. The values can be tabulated as shown in Table 6.

TABLE 6

1. Spectrum Analyzer	50 KHz
2. Beam Convergence	57.6 KHz
3. Vertical Diameter	12.4 KHz
4. Horizontal Diameter	<u>6.8 KHz</u>
Total Frequency Spread	126.8 KHz.

The experimentally determined frequency spread was 125 KHz at half peak height and the value at 5% was 250 KHz. Of course, as the frequency increases, the value of Δf_D increases.

5. Isofrequency Lines. Consider the scattering surface in the direction of the incident radiation. The frequency along the vertical axis is zero. The frequency along the horizontal axis increases linearly with distance (for small distances) on either side of the incident beam. If a hemisphere is constructed about the scattering center with its center at the scattering center and the perimeter of this hemisphere is traversed, the Doppler frequency increases from zero on the vertical axis to a maximum on either side at the horizontal axis then decreases to zero again at the negative vertical axis.

If a plane is cut through this hemisphere parallel to its flat surface and perpendicular to the incident beam and the Doppler frequency is plotted on this plane as a function of the spatial position, a family of isofrequency lines is generated which are hyperbolae with the vertex on the optical axis. The vertical axis is coincident with the conjugate axis of the hyperbolae and the horizontal axis is coincident with their transverse axis. That is, the foci are on the horizontal axis and on either side of the primary optical axis, and in the plane of the velocity vector, \vec{v} .

The eccentricity of each of these hyperbolae is large and approaches

infinity near the vertical axis. In fact, the hyperbolae so nearly approximate a straight line that the negative distortion of the lens causes the curvature to change directions. The resultant experimental determination of the isofrequency lines contains the effects of the lens as well. The net curvature of the hyperbolae is small enough that within the limits of the lens edge a rectangular slit of the same width as the diameter of the limiting apertures can be used in their stead without a measurable increase in the Doppler frequency spread seen on the spectrum analyzer.

6. Frequency Measurement Limits. There are several elements that can limit readout of the frequency information. One of three spectrum analyzers is presently available for use in different regions of the frequency spectrum. For present work this type readout is entirely suitable. Later, other techniques explained below must be considered. One of the available spectrum analyzers (Tektronix 1L20) has an upper frequency limit of 4.2 GHz. This corresponds to a velocity of 2.54×10^6 cm/sec which is well beyond anticipated velocities. It is of the order of Mach 73. A tabulation of limiting factors is shown in Table 7.

TABLE 7

Spectrum Analyzer	Frequency Limits	Velocity Limits (cm/sec)	Velocity Limits (Mach)
Singer SPA-3/25a	200 Hz-25 MHz	$0.121-15.1 \times 10^3$	$3.65 \times 10^{-6}-0.42$
Tektronix 1L10	1 MHz-36 MHz	$605-21.8 \times 10^3$	0.0182-0.657
Tektronix 1L20	10 MHz-4.2 GHz	$6.05 \times 10^3-2.54 \times 10^6$	0.182-76.7

The upper frequency limit of the photomultiplier tube with a 50Ω anode resistor (used to match input impedance of Tektronix spectrum analyzers) and a liberally estimated 50 pF capacitance is 400 MHz. Assuming a linear Doppler shift, this gives a maximum of 242,000 cm/sec or Mach 7.3 which

is not an unreasonable velocity. Of course, associated circuitry, wiring, and electron transit time spread have an effect here, but generally R is the only really controllable factor.

Solid state detectors available that have an upper frequency limit of 1.0 GHz but none of those commercially available have gain. (Types which do have gain are now in the development stage. Hewlett-Packard's pin photodiodes go up to 1.0 GHz and have a quantum efficiency of 0.75, and dark current of 100 pA.) Therefore, it would be necessary to have high gain, wide-band amplifiers or a series of high-gain high-frequency slot amplifiers to use this upper frequency limit. Of course, part of this could be done by using the amplifiers in the high frequency spectrum analyzer which downbeats the high frequency input to a frequency level that can be easily amplified.

High frequency traveling wave tubes have recently been developed. They are, however, expensive and their long term characteristics have not yet been evaluated.

Another possible limit is the wide band C-Cor amplifier. It is perfectly matched to the photomultiplier and spectrum analyzer but its frequency response is 3 db down somewhat above 200 MHz — \pm 0.5 db down at 100 KHz and 155 Mhz. This amplifier in conjunction with a D.C. to 10 KHz amplifier has a gain-bandwidth product of 0.2 THz which is suitable in terms of most gain and frequency applications. If a linear Doppler function is assumed, the maximum velocity becomes 141,000 cm/sec or Mach 3.65, which is an appreciable velocity and probably above the generating capabilities of this study.

The lower frequency limit of the C-Cor amplifier alone is 10 KHz, which would permit 60 db amplification of any signal from 6 cm/sec to 141,000 cm/sec.

7. Noise. Noise, which has proven one of the major problems associated with the studies undertaken here, falls in two categories:

(1) That noise that is inherent in the laser or is introduced into the optical circuit prior to the transformation of the optical signal to an electron current.

(2) That noise that is developed in the photodetector or in subsequent amplifying and detection equipment. Since the electronic noise has proven to be the lesser of the sources, it will be discussed initially.

Since most of the noise is extremely wideband, any optical or electronic filter which removes it also was found to remove most of the desired signal.

(1) Electronic Noise.

a. Photomultiplier noise. With a photomultiplier in total darkness, a certain small amount of noise is detected at the output. The quantity of this noise is a function of the temperature within the photomultiplier. This is true because the source of the noise is random emission of thermal electrons which are then multiplied as they traverse the dynodes of the multiplier. This noise is called dark current and is a form of shot noise. It can be made completely negligible for most work by refrigeration of the photomultiplier, although this method has not been used and will not be for several reasons: the problems associated with securing and utilizing the refrigerant; the safety problems associated with personnel

working around the refrigerant under conditions of no ambient lighting; and the measured values of dark current are so much lower than other sources of noise that it can probably continue to be ignored. This is particularly true when using a spectrum analyzer readout, since this shot noise is spread out over a fairly broad frequency spectrum.

Table 8 lists dark current values for the photomultipliers that have been used on this research and measured at about 25°C.

TABLE 8

Photomultiplier	Dark Current	Equivalent Noise output ($R = 50\Omega$)
DuMont 6911	15 μ A	0.75 mV
Amperex 150 CVP	10 μ A	0.5 mV
RCA 7265	0.8 μ A	0.04 mV
RCA C70038D	1.3 μ A	0.065 μ V

The high voltage power supply for the photomultiplier is highly regulated (0.001%), has high thermal stability (20 ppm/°C), and has good long-term drift characteristics ($\pm 0.005\%$ /hour, $\pm 0.03\%$ /day). The voltage divider consists of zener diodes bypassed by low value capacitance to permit stable operation at both high and low frequencies.

b. Amplifier. The high-gain wideband C-Cor amplifier has an equivalent noise input of 40 μ V and a 50 Ω input and output impedance. The 40 μ V equivalent noise input is spread over a frequency range up to 200 MHz (i.e., the noise is 0.2 μ V/MHz). In terms of the maximum IF bandwidth of a spectrum analyzer equal to 20 KHz, the noise becomes 0.01 μ V. Here the noise is again insignificant.

c. Spectrum Analyzer. If an IF bandwidth of 30 KHz is assumed for a spectrum analyzer, the equivalent input noise (Johnson or white noise) can be

calculated from

$$N = \sqrt{4kT\Delta fR}$$

where N = equivalent noise in volts

k = Boltzmann's constant = 1.38×10^{-23} joules deg $^{-1}$

T = temperature of the input resistor in degrees Kelvin $\approx 300^{\circ}\text{K}$

Δf = frequency range of the signal of IF bandpass of the instrument

R = Value of input resistance in ohms.

Table 9 contains the noise values for the spectrum analyzers that are used.

TABLE 9

Spectrum Analyzer	Max IF Bandwidth, Δf (Typical)	Input Impedance Z_i	Equivalent Noise
Singer	20 KHz	72 Ω	0.155 μV
1L10	1 KHz	50 Ω	0.0288 μV
1L20	100 KHz	50 Ω	0.288 μV

It should be noted that the noise figures quoted in Table 9 are worst case values. As the IF bandwidth is narrowed, the noise decreases as the square root of the bandwidth. In no case has this white noise ever been the limiting factor, even though it can be seen on the 1L10 and 1L20 spectrum analyzers.

d. Stray Electrical Pickup. Most extraneous pickup is eliminated by the use of shielded cables necessary at high frequencies. Under certain conditions there is some R.F. feedthrough from the laser R.F. supply, but since it is a narrow frequency, it does not affect the readout in the general case. However, it prevents observation of data on an oscilloscope because of its high continuous value in the time domain.

(2). Optical Noise.

a. Laser. The largest single source of noise is the laser itself. A more thorough discussion of this noise will be given in the appendix. It consists basically of three types: mode noise, plasma noise and spontaneous-emission noise.

The mode-interaction noise in the particular 50 mW laser that is being used is well defined, relatively stable and near zero frequency. Therefore, it has not introduced problems in readout on spectrum analyzers.

The plasma and spontaneous-emission noise have continuously been present. In the 0.8 mW laser used in initial studies the best signal-to-noise ratio ever obtained was 4 to 1. In this case, the spontaneous noise would be expected to be high. However, in the RF stabilized 50 mW laser the radio frequency waveform as well as strategically located ceramic magnets about the plasma tube are supposed to reduce the noise significantly. It has not been possible to significantly reduce this noise. With about ten times the power (the output of the SP 125 is 74 mW) of the small laser the maximum signal-to-noise ratio is 13 to 1.

b. Extraneous Coherent Light. All the components in the system scatter varying amounts of laser light. The output reflector of the laser cavity scatters a great deal. This reflector was recently replaced because the anti-reflection coating had been etched, which caused a significant increase in the scattering. Since the input beam travels a rather large distance before it reaches the rotating disc, much of the light scattered by the laser reflector may be eliminated by placing apertures along the path of the incident radiation. However, there is some forward scattered

light that transverses the apertures along with the incident beam.

Scattering also occurs from all reflectors, the surface-surface interfaces of the compound lenses, and the interfaces of the beam splitter and of the optical path length equalizer. The net result is to give a D.C. optical bias which contributes nothing to the signal but causes a higher background noise. This effectively lowers the modulation index of the heterodyned signal. Some of this noise can be removed by limiting the portion of the photomultiplier cathode geometrically available to scattered rays.

c. Incoherent Light. Ambient light also contributes to the D.C. optical bias at the cathode of the photomultiplier. This light comes from the plasma discharge of the laser, the hot cathode of the laser, fluorescence of cathode ray tube screens, scale light on cathode ray tubes, pilot light on auxillary measuring equipment, and room light.

The most important source of this noise (room light) has been eliminated by the unsatisfactory expedient of working without lights on, posing a rather severe safety hazard. Pilot lights have been removed and the hot cathode of the laser was covered, eliminating another important source of incoherent light. Because of overheating, the laser cannot be covered for the long periods of time during which experiments are in process, leaving the plasma light as a major source of incoherent light noise. The light from the cathode ray tubes and scales can be minimized, but of necessity must remain on. Vacuum tubes may be mechanically covered.

Other techniques are also used to help eliminate this incoherent light. Of course, the small photocathode area available to the coherent

light helps to minimize noise of this type as well. In addition, an optical filter (low frequency band pass) chops off any light with $\lambda < 6000\text{\AA}$. Selective filtering of room light coupled with filtering at the photomultiplier may alleviate the safety problem mentioned above.

All of this difficulty with incoherent wideband light stems from a property of the photomultiplier itself with respect to light of wavelength 6328\AA . The photomultiplier is less sensitive to the 6328\AA line than to any other shorter wavelength down to about 4500\AA depending on the particular sensitivity of the photocathode. For some of these wavelengths it is more sensitive. Since the desired wavelength is narrow and the photomultiplier is not sensitive to it, the integrated value of the photomultiplier sensitivity is many magnitudes greater than for the wide band light from black body radiators. That is, it takes little light spread over the white light spectrum to which the P.M. tube is sensitive to completely swamp the narrow band centered about 6328\AA .

d. Misalignment or Non-coincidence of Heterodyned Beams. If the beams to be heterodyned are not of the same size or are aligned such that they do not form coterminous discs on the photomultiplier, an effective optical D.C. bias is again introduced. This occurs any time that light is present that is not being heterodyned with other light. It is not difficult to get a factor of two increase in signal-to-noise by extra careful alignment as opposed to careful alignment of the beams. It can be seen that the size of the limiting apertures are critical as far as minimizing noise is concerned.

e. Unbalance in Heterodyned Beam Intensities. If the intensity of the

two beams are not the same when they impinge on the photocathode, the modulation index deviates from unity and the noise increases. This can be seen easily by beating the unattenuated light from the back of a laser with one of the scattered beams. In this case, only extremely careful alignment can pull the signal out of the noise.

f. Fine Lobe Structure of the Scattered Radiation. As predicted by Mie scattering theory, the large lobes are made up of many finer lobes. If the two cylindrical beams defined by the limiting apertures are cut with a plane perpendicular to their axes and the scattering surface is stationary, the two cylindrical beams produce two $3/16$ inch diameter discs at the plane of intersection. The internal makeup of these two discs is a complex (and visually uncoordinated) series of light and dark splotches corresponding to the mini-lobes and valleys respectively. The internal patterns of the two discs are in general completely different. When the two discs are superimposed such that their perimeters are coincident, there are significant areas of dark in disc #1 that fall on either dark or bright areas of disc #2 and vice versa. Of course, the superimposed dark areas produce no signal or noise. At the other extreme, the bright areas superimposed on dark areas produce all noise and no signal. If an area from each of the two discs have different intensities, the modulation index and noise generated is comensurate with their intensity ratio. Statistically there are areas on the two discs that are of equal intensity and, upon superimposing, the discs produce a modulation index of unity. It can be seen that the heterodyne efficiency of the system is somewhat low and that there is a large amount of noise introduced as a result.

The actual efficiency depends on the fine lobe structure developed at the scattering surface. As the scatterer moves, other discs appear with completely different internal structures leading to an infinite number of heterodyne combinations that are impossible to treat analytically.

Attempts have been made to integrate the lobe structure with absolutely no success. Care must be taken in this process to preserve the frequency profile of the two beams to enable cancellation of the frequency spread. The most obvious technique for doing this is to focus the two beams together onto the photocathode of the photomultiplier. As discussed above, the resultant current was lower than before focusing. Another technique that should have worked in theory was to rescatter the two beams using extremely small scattering particles located close to the photocathode. This method also did not work well enough to continue using it.

8. Intensity and Signal-to-Noise Ratio.

The lack of intensity, or more accurately a low signal-to-noise ratio, has been a difficult problem to date. The noise problem and its causes were discussed in the previous section. In this section some of the limiting factors on intensity will be discussed. Signal-to-noise ratio is defined here as the ratio of the signal height from the base line to the noise height to the base line.

The fundamental limit on signal-to-noise is obviously the output of the laser itself. Since the noise carried along with the laser radiation is optical, the signal/noise relationship is linear except for secondary phenomena which introduce non-linear effects. The laser used in initial studies had an output of 0.5 mW. After a higher power laser became available

(Spectra Physics 130B with an output of 0.8 mW) it was used. For some extremely critical determinations it was possible to borrow a 10 mW laser for short periods. This was done over a short period of time, but because of the severe inconvenience caused to the people normally working with the laser, this was soon discontinued. The use of the 10 mW laser did facilitate certain studies because of the higher signal-to-noise ratio. Since the 10 mW laser was mounted on a granite table, this also helped minimize vibration problems.

The use of a Spectra Physics 125 laser with an output of 72 mW at 6328 Å has permitted a gain in signal-to-noise of a maximum of 13 to 1. By mounting the optical system on a granite table, signal fluctuation caused by room vibrations have been minimized. Application of rf power increases laser output by 35.4%. All of the lasers used were diffraction limited and had plane polarized outputs.

Each of the system components contribute to the decrease in intensity. These components were picked to maximize intensity. Of course, the biggest transition in intensity occurs at the scattering medium where an incident beam of about 40 mW power is transformed into countless scattered lobes of power in the nanowatt range. Except for the small absorption loss at the scatterers, the sum of the powers of the lobes will be equal to the input power. Assuming that the scattered intensity is evenly distributed throughout the back hemisphere, each limiting aperture intercepts about 4 microwatts of power. Therefore, there is an automatic stepdown of 10,000 in intensity from the incident beam, making it imperative that the following and preceding components have maximum efficiency. All power levels greater

than 0.1 mW were measured by a spectra Physics Model 401 power meter.

(1) Component Reflectivity.

Several reflectors are necessary in the optical circuit. Their maximum measured efficiency is 89%, the other 11% being absorbed. This value is accurate for both aged gold plated glass and for right angle prisms in which the reflection occurs at the hypotenuse plane within the glass. Aluminum mirrors absorb any amount from 15% to 32%. Attempts will be made to approach 5% absorption on gold coated surfaces following a recently announced technique (6). It is particularly important to maximize the reflection from the mirror in one leg of the mixing arrangement to help maximize heterodyne efficiency.

(2) Lens.

The original lens used in the optical network for early experiments had a focal length of 8 inches and a diameter of 5 inches. These dimensions were ideally suitable for the proposed studies. However, the loss of light being transmitted through the lens was rather high because of the deterioration of the anti-reflective coatings and inhomogeneities in the lens.

A corrected lens from a Tropel 4 inch collimator with a focal length of 40 cm and a 10 cm diameter with high quality anti-reflective coatings has now been substituted (see Figure 7). It has a transmission of 92.9%.

(3) Beam Splitter.

The beam splitter is the weak point of the portion of the optical system for the scattered light. The original beam splitter used in the system had the following characteristics: absorption 54%; reflection 28%;

and transmission 18%. The modulation index is 0.644.

These figures can be used to discuss some problems involved. Consider for a moment that all other aspects of the two beams impinging on the beam splitter are ideal; i.e. they are of uniform intensity, of equal intensity, and of the same size. More than half of each beam is immediately lost by absorption. Therefore, the heterodyne current is cut by a factor of two. In addition, only 18% of beam #1 beats with 28% of beam #2. Therefore, there is a large D.C. optical bias introduced which cuts down the heterodyne current even more and introduces a large amount of noise.

In addition, 18% of beam #2 and 28% of beam #1 is thrown away by being perpendicular to the beam above which enters the photomultiplier. Attempts have been made to use this beam as well (effectively doubling the signal) but with only partial success. At times the heterodyne current is doubled; at other times it is cancelled. The cause of this phenomenon has not been ascertained yet. It cannot be a phase difference since the wavelength (considering a 10.0 MHz Doppler frequency) is of the order of 33 meters and the path difference between the beams leaving the beam splitter is about 3 cm. This indicates that the phase difference could not be more than 0.1 or about 0.1 degree out of 360 degrees, which is hardly sufficient to provide complete cancellation.

By use of neutral density filters the possibility of severe photocathode saturation has been eliminated and by carefully selecting another beam splitter, the efficiency has been increased. This beam splitter is apparently dielectrically coated and has the following salient values: absorption 8.9%, reflection 41.1%; and transmission 50% for one beam;

and absorption 21.7%, reflection 28.3%, and transmission 50% for the other beam. The modulation indices are 0.822 and 0.566 respectively.

There has been a significant gain in efficiency of heterodyning. However, there is still a large amount of light that does nothing but contribute to the noise level. Of course, the ideal beam splitter would have 50-50 transmission-reflection for both beams. Such a device is apparently unobtainable.

It is not too difficult to match transmittance-reflectance for one beam, but the absorption becomes large and the match does not hold for the other beam.

(4) Longitudinal Mode Effects.

The S.P. 125 laser operates in many longitudinal modes, which change the interference efficiency of two beams that are permitted to interfere (in this case called heterodyning). If the heterodyne efficiency is plotted versus the number of laser cavity lengths between the two beams, a curve like that in Figure 8 is obtained. If the two beams have the same length ($\Delta = 0L$) the interference is a maximum. This decreases rapidly as the difference in path lengths increases. At $\Delta = 2L$ the interference is again a maximum as it will be at every interval of $2nL$ where n is an integer and L is the cavity length of the laser (148 cm). In the system used in this study, the value of Δ is such that the interference efficiency is down to about 60%. Two methods for correcting for this difference are readily obvious. First, Δ can be made to equal zero by folding the shorter beam with two mirrors to increase its path length to correspond to the other beam path length. This introduces two extra mirrors which

each cut down beam intensity by 11%. Two mirrors are necessary to fold the rays back to their original orientation to again eliminate aperture size dependent frequency spread. This is not a good approach. Another technique is to introduce a material of high refractive index to make the shorter beam have an effective longer path length. To do this, the introduced medium must have a high refractive index to be reasonably short. This introduces severe light losses at the glass-air interfaces. If the refractive index is kept at a reasonably small value to minimize interface losses, the medium must be rather long. Glass rods with plane-parallel faces are expensive. The length needed for material of $n = 1.5$ is about 7 cm. The technique that was used was to join two small right angle prisms to a large right angle prism with Canada balsam to give a 7 cm retarding medium.

(5) Beam Spread Effects.

If one of the scattered beams is more or less divergent than the other (which is likely since the lens is not corrected for light transversing it antiparallel to the incident radiation and since the beams are of different lengths), the signal-to-noise ratio is decreased. This problem is corrected by the procedures outlined for correcting path length difference.

(6) Optical Filters.

An optical filter placed in front of the laser helps cut out some of the noise but it also contributes to a decrease in light available for scattering. Another filter placed immediately in front of the photomultiplier helps attenuate noise but also attenuates the desirable light input. The bandpass filters are a CS 2-63 with 78.6% transmission and a CS 2-61 with 83% transmission.

(7) Spatial Filters.

Spatial filters are generally selected for efficiency. The spatial filters located throughout the optical network are greater than 99% efficient. The area of the limiting apertures is directly related to the total intensity within limits of spatial coherence.

(8) Photomultiplier.

The particular line in the optical spectrum at which the He-Ne laser operates is undesirable in relation to photomultiplier sensitivity. Any photocathode is at low values on its response curve at 6328\AA . Photocathodes that operate in this range have inherently low quantum efficiency; therefore, their response is low initially. The values for the photomultipliers in use on this research are given in Table 10. An emitter follower was used between the photomultiplier and spectrum analyzer in earlier studies at low frequencies to permit matching the maximum possible load to the low Z_i of the spectrum analyzer.

TABLE 10

Photomultiplier	Quantum (%) Efficiency	Radiant Sensitivity(A/V)	Per Cent of Maximum Response	Wavelength of Maximum Response
DuMont 6911	0.36	1,750	70	8000
Amperex 150 CVP	0.36	6,300	70	8000
RCA C70038D	25.0	3,750	75	5500
RCA 7265	18.0	1.2×10^6	40	4200

Each of these tubes is more efficient and has higher sensitivity at shorter wavelengths (except for the S-1 response which is maximum at 8000\AA).

Quantum efficiency, radiant sensitivity and peak operation are in general mutually exclusive. The RCA C70038D has the highest quantum efficiency

and operates higher on the spectral response curve but its radiant sensitivity is low. The RCA 7265 has relatively low quantum efficiency and operates lowest on the spectral curve but has the highest radiant sensitivity of any tube made.

The RCA C70038D has a smaller photocathode area (0.65 X 0.5 inch) causing it to have little transit time spread. Therefore, it has been used for high frequency work. A special voltage divider has been constructed which permits a flat frequency response from D.C. to over 400 MHz (depending upon the value of load). This divider is made of a high tolerance zener diode (1N4758A and 1N4759A) matched to give equal voltage drops at each stage and with each stage bypassed by a small 1000 pF capacitor. Leads are as short as possible. This configuration not only permits high frequency response but also prevents loading of later dynode stages.

The other photomultiplier tubes have their own specialities with the 6911 being the work horse of early low frequency studies. The 7265 will be used in studies where the input signal is extremely low because of its inherently high radiant sensitivity. All of the photomultipliers are electrically shielded. This shield also serves as an optical shield. In addition, the C70038D is double shielded. An inner shield of ferromagnetic metal is tied to the photocathode and acts as a magnetic-electric shield. A second concentric shield acts as an optical shield and an electrical insulator. The 7265 will be mounted in the same manner.

The intensity level can be increased also by bringing both primary beams in at other than 90° and multiply reflecting them.

(9) Amplifier.

A wideband C-Cor amplifier with 60 db gain was used between the photomultiplier and spectrum analyzer. It had an input and output resistance of 50 ohms and was matched to the 50 ohm load of the photomultiplier and 50 ohm input impedance of the spectrum analyzer to minimize signal loss at high frequency. Fifty ohm cables were used and kept as short as possible. This amplifier responded to rather rapid pulses (15% ringing for 1 nsec input step) because of its 3.0 nsec rise time.

(10) Polarization Effects.

The study of polarization effects is not complete but it is known that the polarization mode of the incident beam or of the scattered beams has some effect on the center frequency of the heterodyned signal. The scattered radiation is polarized to an extent and each individual lobe can be completely polarized. There appears to be a change in the frequency-intensity curve with changing polarization. In particular the amplitude of this curve changes. There is a problem related to this study because of the ability of the beam splitter to polarize beams impinging upon it. According to Lee's criteria, the maximum heterodyne efficiency occurs when the major axes of the polarization ellipses of the scattered radiation are aligned. This can be done by rotating the major E component of one leg of the heterodyne arrangement.

9. Volume Scatterers.

Initially plans were made to use the colloidal type characteristics of rotating cylinders of polyethylene. However, as was discussed earlier, this particular polymer follows laws of dependent scattering and as a result

is unsuitable for an analogue of most flowing systems containing impurities.

As an alternative, other plastic systems which are liquid or semi-liquid before curing were investigated. The goal would be to suspend scattering particles in these optically transparent media and permit the plastic to cure forming a volume scatterer. The plastics for this purpose were studied from a superficial standpoint independently of the particle studies.

The particles that were considered for this use were:

- (1) The pigment from the diffusely scattering point discussed in detail above.
- (2) The Teflon-Freon suspension used by MSFC.
- (3) A suspension of Teflon in water commonly called "liquid Teflon".
- (4) Extremely small glass beads (suffering from disadvantages covered above).
- (5) Monodisperse Polystyrene Latex or Styrene Divinylbenzene Copolymer.

These plastic spheres are available from Dow Chemical Company only in limited quantities. In the monodisperse plastic, the presently available spheres are in the lower Mie range ($0.09 - 1.099\mu$) with its low scattering efficiency. The other plastic is available in severely truncated polydisperse form that spans the Mie scattering region ($6-100\mu$) but has a particle size distribution too wide to be used (e.g. $6-14\mu$, $12-35\mu$, $25-55\mu$, $50-100\mu$). Dow's availability of other sizes is strictly contingent upon the success of its effort for making them at a given time. According to Dow the particles are clear giving them the disadvantage of any clear particle. However, the original source of this information insists that they are

white and opaque. Their density ($\rho = 1.05$ g/cc at 20°C) is comparable to that of water, making them suitable for following turbulent flows. Dow says they have optical properties approximating those of bulk polystyrene ($n = 1.592$). They are sold in 15 ml vials and suspended in deionized water. They exhibit a slight negative charge. Although none of the particles discussed above have been eliminated completely, the first three have the highest backscattering intensity and are more suitable for this study.

Other possible sources of scattering centers which have not been studied in great detail but are discussed in the literature are the photolysis of iron carbonyl in air which produces a highly dispersed reproducible and stable aerosol (7), the precipitation of sulphur particles from a thiocyanate solution, and the use of a vibrating reed to form particles from a liquid or semiliquid which are immediately solidified. All of these techniques have their disadvantages.

The suspending media considered for containing the particles were:

(1) Clear epoxy.

All epoxies checked were not sufficiently clear to be used. They have a significant amount of yellow color which absorbs in the red portion of the spectrum. In addition, the curing cycle was rather poorly defined, making it difficult to get uniform particle distribution with no air bubbles.

(2) Silicones.

Attempts were made to secure single solution plastics in the silicone family. This would simplify curing and make it easier to get uniform particle distribution. Dow Corning has several moldable silicone compounds (two solution) which have excellent optical properties. Stylgard 184 resin

has the best optical properties of standard resins and has a refractive index of 1.43. Dow Corning XR-63-488 is slightly better because of selected resin. The two are in short supply and therefore a slightly less desirable (according to Dow) resin, Dow Corning XR-63-493 was obtained. According to our tests, it has the optical qualities of relatively expensive optical glass but with lower refractive index.

In addition, a two component silicone compound was obtained from General Electric. This compound has a refractive index of 1.41 and is more rigid than the compounds above. It is designated as G.E. RTV-615A. Its transmission characteristics are lower in the uncured state because of its straw color, which according to G.E., becomes clear after curing. This has not been checked. All of the silicones have a rubbery consistency, which indicates that their dimensional stability is poor under stress. At a constant motor speed this will not be too important.

(3) Polyester Resin.

A two-component polyester resin which hardens into a rigid plastic upon curing was also purchased for studies. It is exceptionally clear but it is rather difficult to control its curing cycle. Its refractive index is about 1.53, which is a little high but acceptable.

E. Conclusions.

Figure 9 shows the result of the evaluation of the experimental apparatus. The light source, S, is an S.P. 125 laser with output of 72 mW. The beam passes through a bandpass filter and is reflected onto an optical bench by prism, P_1 . The incident beam is focused by lens, L, with a diameter of 4 inches and an f-number of $f/4$, onto a rotating disc coated with

high-diffusivity white pigment with particle sizes in the Mie scattering region. The resultant intensity lobes are scattered back through the lens and two cylindrical segments symmetrical to the incident beam are defined by two 3/16 inch apertures. One beam is reflected by prism, P_2 , onto a beam splitter, B, with 50% transmission and 28.3% reflectance. The other beam traverses an optical retarder, R, and impinges upon the same beam splitter which mixes the two beams optically into two other beams (containing components of both original beams): one which directly impinges on the photomultiplier cathode, C, and one which is reflected by prism, P_3 , onto the cathode. The Amperex photomultiplier heterodynes and multiplies the signals which are displayed on a 1L20 or Singer spectrum analyzer, A, depending upon the Doppler frequency and upon the data desired.

Signal-to-noise has been of major concern; the maximum attainable was 13/1. A large amount of the noise originates in the laser. The photomultiplier's higher sensitivity to broad band light than to narrow band 6328Å light also contributes to the noise.

Particle size and particle size distribution contribute a negligible amount to the spread in Doppler frequencies. The major contributions to this frequency spread (which is about 150 KHz) are the spectrum analyzer, the horizontal and vertical sizes of the focused light spot, and the angle of convergence of the incident beam.

The intensity of the signal is dependent upon the shape, size, distribution, color, refractive index, and size distribution of the scattering particles. The conductivity (metal versus insulator) determines the polarization mode of the scattered light.

The frequency limit is determined by the 2000 MHz, 3 db point of the amplifier. The intensity limit is defined by the Johnson noise level to be about 0.2 μ V of signal.

The heterodyne efficiency is determined by minilobe distribution within the two scattered beams, by their path length difference, by the beam splitter efficiency and symmetry, and by Lee's criteria. The maximum efficiency obtained has been less than 0.5.

III. Future Work

A. Polarization effects. The study of polarization effects will be continued, including the determination of the orientation effects of the \vec{E} vector of plane polarized light upon the characteristics of the scattered light. The rotation of the polarization vector is accomplished by use of a spectra Physics Model 310 polarization rotator. Another laser with unpolarized output can be used to check the other extreme of incident beam polarization characteristics. Mie theory predicts that either plane polarized or unpolarized light or any other polarization mode of incident radiation will give elliptical polarization of the scattered radiation if the scattering occurs from a non-conductor. In metals ($\sigma > 0$) the scattered light preserves the polarization mode of the incident radiation.

By use of polaroids and photodetector, the polarization ellipse of the scattered beams can be plotted for various conditions of incident radiation. Alternately, the incident beam conditions could be changed and the output of the experimental apparatus could be optimized in situ. The latter approach would not give intermediate data.

According to theory, the ellipses of polarization of the two scattered

beams should have the same ellipticity but would be mirror images. This predicts a case in which the major axis of one would be coincident with the minor axis of the other leading to a reduction in heterodyne current as a function of the ellipticity of the polarization ellipse. In the worst case ($\sigma = 0$ and incident plane parallel polarized incident light) the current would be zero. In the best case the scattered light would be either circularly polarized or unpolarized and the heterodyne current would be maximum. Fundamentally the heterodyne efficiency is a function of the cosine of the angle between two plane polarized beams. This is modified some by deviation from the plane polarization condition.

The condition of mirror imaged ellipses can be corrected by use of the polarization rotator in one of the scattered beams. However, if the ellipticity of the ellipses is small and/or the degree of rotation of the major axes is small in the positive and negative directions respectively, the gain in heterodyne current may not be sufficient to offset losses in the polarization rotator, which are somewhat less than 10%.

B. Volume Scattering.

The study of the behavior of three-dimensional scatterers (volume scatterers) is necessary for a full understanding of the behavior of a system and its application to fluid behavior. It is not known if the scattering lobes can be shaped to be a maximum along the incident axis as in surface scatterers.

Plastic systems have been considered and several have been purchased for studies as discussed before. These studies will involve the suspension of scattering particles in optically clear media which hold the particles

in place. One problem may arise in the reflection from the surface of the optical flat on which the scattering suspension is mounted and at the interface of the flat and the scattering medium. If the selectivity of the optical system is not sufficiently high to reduce the reflected light received to a negligible value, there will be interference from the surface light.

The polyester resin with suspended scatterers described before and the silicones (if the motor speed is constant) will be used to study the scattering characteristics of volume with a constant position and velocity in space (approximating laminar flow). The effective size of the volume, its shape, and its other salient features will be determined.

By modulating the speed of the rotating silicones, a well defined-periodic measurement of pseudo-turbulence can be measured, which is a function of the flexibility of the cured silicone. As the motor speed changes there is a characteristic displacement in the location of particles which will be periodic with modulation frequency. This should permit a better understanding of the behavior of a true turbulent flow.

After the culmination of the volume studies would be a good time to study the readout of two and three-dimensional Doppler frequency shifts. By using three sets of different non-planar observation angles (θ_1 , θ_2 , θ_3), it will be possible to check the reliability of using a single photomultiplier to study three different velocity components. Since any three non-planar coordinates can be orthogonalized, this could possibly give a measure of the three velocity orthogonal components of a three-dimensional velocity vector, \vec{v} . The experiment would only check out a technique and would

probably have no validity as far as the true turbulent flow is concerned.

An important question to be concerned with in volume scattering is what percentage of the detected radiation originates from the $1/e$ (63.2%) power portion of the focused spot and what portion comes from outside this region or from the two cones (for the 40 cm focal length lens these are approximately cylinders) in front of and behind the focal point. Determination of these values will give the effective scattering volume of the system. Acceptance of significant quantities of radiation from either source will cause loss of resolution in the determination of the turbulent flow pattern.

Conversely, the resolution can be too high. If the focal point were extremely small, the scattered radiation would have such wide dynamic excursions that the data would be useless. It would probably be possible to get a variation in velocities from a maximum in the direction opposite to the flow direction to a maximum in the flow direction, all within the specified readout time. There could possibly be a slight peak at the frequency corresponding to the average velocity, but in general the data would be displayed effectively as a broadband noise spectrum. Therefore, the chief problem is judicious selection of parameters to permit understandable readout of any data that may be present in the heterodyned backscattered radiation.

C. Fluid Flow.

The next step would be to apply the information obtained to date to laminar liquid or gas flow in recirculating systems using the contaminant selected in the volume scattering experiments. Since no additional

contributions are expected in the laminar flow region, the next step would be to study turbulent gas flow in a closed system using the same Mie scatterers.

In turbulent flow the problem becomes more complicated. Since the direction of flow is time variant and unknown at a given time, the velocity vector, \vec{V} , must be measured to completely analyze the flow distribution at the desired point. The simplest method to measure \vec{V} is to measure its orthogonal coordinates in cartesian 3-space. Of course, it should be theoretically possible to use other than orthogonal components as long as their direction cosines are accurately known.

All of the data taken to date has been necessary in order to understand the contribution of different system parameters to the data. This complex problem as delineated in the foregoing report was anticipated and was the basis for reasoning that precluded the direct assault on three-dimensional turbulent fluid flow. By following this logical pattern, a firm basis has been built on which to study the extremely complex problem of time-variant (turbulent) flow. It is anticipated that one and two-dimensional measurements of turbulent flow will yield incomplete data of nebulous value. Not until the complete three-dimensional ensemble is viewed will the analysis of turbulent flow be completely understood. At this point an anemometer will be necessary to help correlate the data obtained from the optical measurement of \vec{V} .

In fluid studies S/N ratio becomes extremely important. Possibly by the use of Fresnel optics a greater amount of light along an isofrequency line can be collected. Perkin-Elmer Company makes optical coatings that

transmit 95% of impinging light through 25 glass-to-air interfaces. This coating coupled with special high reflectivity mirrors should permit a rather large increase in intensity. These will be used only as a last resort because of the cost involved.

The proposed three-dimensional studies of turbulent flow would be the final step in the logical process outlined before. Many of the problems of one and two-dimensional studies will carry over to this culminating study. However, problems are expected which are solely a function of the three-dimensional system. For example, optical crosstalk among the three readout channels cannot be completely discounted. In addition, the electronic readout devices will be a problem. As a first approximation three photomultipliers and three spectrum analyzers will be necessary. However, with certain techniques it might be possible to develop a system utilizing only one or two readout devices. The problems here would be caused by the possible interference between the signals as seen on the spectrum analyzer and the difficulty of ascertaining which coordinate velocity a given spectral distribution represents. This would be a severe problem if the maximum velocity were alternating from one axis to another as it would almost certainly do in a turbulent system. The next section discusses other readout techniques in detail.

D. Readout of Data.

Initial experiments will be performed using a spectrum analyzer readout. If the turbulence is intense or if the frequency spread is large with respect to the velocity spread, other techniques will be necessary since the wide frequency spread (corresponding to a wide velocity distribution)

will not be translatable on a standard spectrum analyzer readout.

An alternative readout technique would involve translation of the time variant frequency into an amplitude function in which the variation of amplitude with time could be linearly related back to frequency and therefore to the velocity of the particular scattering volume. Of course, the proper linear relationship could be maintained if the scattering volume were sufficiently small to minimize the possibility of receiving data from more than one eddy at a given time. This criterion should not be too difficult to meet since the sampling volume can be made small. According to Foreman et al. (4), the value of the scattering volume is of the order of 10^{-6} mm^3 .

Another limitation would be the maximum readable frequency as determined by the characteristics of the filter used to generate the linear amplitude response. As the frequency increases, the response will level off and become flat, destroying the known relationship between the amplitude and frequency. The block diagram of such a simple circuit would be that shown in Figure 10.

The output discussed above is effectively an analogue signal. A more direct method of determining the amplitude-frequency relationship at any given time would be the use of a digital computing circuit. In this case the signal from the high gain amplifier would be fed to a digital computer which would sample the signal for a given length of time, determine the number of cycles occurring during this time, and read out the frequency or even the velocity directly.

Frequency limits are also associated with the use of a digital computer.

If all the cycles are counted, the clock time required for the computer to count a 400 MHz signal would be 2.5 nanosecond, which is below the limit of the present generation of high speed computers.

Of course, other techniques could be used to count at somewhat faster rates but with a resultant loss in accuracy. For example, an independent logic scheme could be used which, upon reaching a given number of counts, would send a pulse to the computer. The residue remaining after the sampling pulse terminated would be lost to the computer and would result in an error in the frequency determination. The magnitude of the error would depend upon the number of samples taken and upon the number of cycles included in an equivalent computer input pulse.

Another technique would be to mix the sampled signal with a local oscillator to down beat the frequency to one comensurate with the clock frequency of the digital computer. This would be similar to techniques used in high frequency counters. In this case the basic accuracy of the direct computer read-in would be maintained.

The computer could be used to give a statistical distribution of the velocities at the given sampling volume. That is, over a period of time the number of samples corresponding to a given frequency would be summed and a resultant curve plotted either in digital form or through an interface into analogue form from an analogue computer. Of course, this would give a small time delay in obtaining the necessary data, but the desirability of having both the velocity-time information and the velocity distribution information in a given segment of time would offset this minor difficulty.

The velocity distribution could be ascertained by using a multi-channel analyzer without the digital computer. In this case there would also be a frequency limit that could be overcome by either of the methods suggested above. Again there would be a time delay in getting a reading while the equipment sampled the velocities. However, this pulsed means of sampling would probably have no more disadvantages than attempts to measure the data continuously.

REFERENCES

- (1) Foreman, J. W., George, E. W. and Jetton, J. L., "Gas Velocity Measurement Using Scattering Techniques," Technical Note R-178, January, 1966.
- (2) Mie, Gustav, "Beitrage zur Optik truber Medien, speziell kolloidaler Mettallasungen, *Annalen der Plysik*, 24, 372-445 (1908).
- (3) Condon, E. U. and Odishaw Hugh, (eds.), Handbook of Physics, Optics, Light Scattering, McGraw-Hill, 6-122 (1958).
- (4) Lee, Cullen Q., "An Investigation of Photoelectrically Heterodyned Coherent Light," Astrionics Research and Development No. 2.
- (5) Hass, Georg and Ritter Elmar, *J. Vac. Sci. and Tech.* 4, 71 (March, April, 1967).
- (6) Jander, G. and Winket, A., *Kollois-Z*, 63, 5(1933).
- (7) Spectra-Physics Laser Technical Bulletin Number 5, p.8.

GLOSSARY

i	=	current generated in the photodetector
E	=	amplitude of the optical signal
α_0	=	first constant of Fourier expansion
α_1	=	second constant of Fourier expansion
λ	=	vacuum wavelength of incident radiation
d	=	diameter of the scattering particles
\emptyset	=	angle of incident radiation
\emptyset'	=	angle of reflected radiation
r	=	particle radius
I	=	intensity of scattered radiation
I_0	=	intensity of incident radiation
v	=	volume of the scattering particle (scattering volume)
k	=	a proportionality constant
I/I_0	=	scattering cross section for random scatters
θ	=	observation angle
$I(\theta)$	=	intensity as a function of observation angle
N	=	Number of scatterers per unit volume
n_0	=	refractive index of medium
α	=	polarizability tensor
X	=	distance from scattering center to optical receiver
T	=	scattering coefficient
λ'	=	wavelength of radiation in medium

$P(\theta)$ = degree of polarization with observation angle

m = ratio of refractive index of scatterer to that of medium

n_1 = refractive index of scatterer

y = coefficient relating particle size to wavelength

f_D = magnitude of the Doppler frequency shift

v_n = velocity along a given coordinate system at the focal point

λ_o = vacuum wavelength of the incident radiation

ψ = angle between the velocity component and the incident radiation

θ = observation angle relative to incident radiation

$f_D(\text{Tot})$ = center frequency read on the spectrum analyzer

V = fluid velocity

R = Reynolds's number

D = tube diameter

ρ = density

APPENDIX I

Optical Scattering by Spherical Particles

Jack G. Dodd

The following is a condensation and summary of relevant material in 'Light Scattering by Small Particles', Van de Hulst, Wiley & Sons, first ed. (1957).

This discussion will be restricted to scattering by uniformly sized, homogeneous, non-absorbing spheres (water droplets). This is one of the few completely soluble cases.

Consider the scattering diagram shown in Figure 11. For N particles/unit volume and incoherent scattering the intensity at r is

$$I = \frac{NV}{4\pi r^2} I_0 F(\theta, \phi) \quad (1)$$

where I_0 is the incident wave intensity, K is the wave number $2\pi/\lambda$, and $F(\theta, \phi)$ is the scattering function which depends upon the details of the polarization of the incident beam and the nature of the particles. For linearly polarized incident light and spherical particles,

$$F(\theta, \phi) = i_2(\theta) \cos^2\phi + i_1(\theta) \sin^2\phi \quad (2)$$

where

$$\begin{aligned} i_1 &= |S_1(\theta)|^2 \\ i_2 &= |S_2(\theta)|^2 \end{aligned} \quad (3)$$

Now define

$$X = Ka, = \frac{2\pi a}{\lambda} \quad (4)$$

where a is the radius of the scattering particle, and

$$\rho = 2x(m-1) \quad (5)$$

where m is the index of refraction. The only simple cases are those in which $m \sim 1$ and either X or ρ is either extremely large or extremely

small. In scattering of 6300Å light by water spheres of radius ~ 3 microns, a reasonable case for discussion here, $X \sim 30$ and $\rho \sim 20$. This corresponds to the region usually characterized by the term "anomalous diffraction". To proceed further will lead to extreme complications unless it is now assumed also that $|m-1| \ll 1$.

This is not really true for water droplets; $m-1$ is 0.33 which is certainly comparable to unity. However, the qualitative results obtained by assuming $m-1 \ll 1$ are comparable to those obtained from strictly correct calculations for sufficiently large spheres. (I-1)

On this assumption, it is found

$$S_1(\rho) = S_2(\theta) = x^2 A(\rho, z), \quad (6)$$

$$\text{where } z = x\theta \quad (6')$$

Substituting in Equations 2 and 3, the following is obtained

$$I(\theta) = \frac{k^2 a^2 |A|^2}{r^2} I_0. \quad (7)$$

That is, the scattered light is polarized in the same plane as the incident light and the scattered intensity $I(\theta)$ is independent of ϕ . (I-2) The function $A(\rho, Z)$ is given as an integral

$$A(\rho, z) = \int_0^{\pi/2} (1 - e^{i\rho \sin T}) j_0(z \cos T \sin T dT) \quad (8)$$

where J_0 is the Bessel function of zero order and T is the dummy variable of integration. This integral is not expressible in terms of elementary functions. Numerical values calculated show an oscillating but rapidly decreasing function of the scattering angle θ . The attached altitude chart (Figure 12) shows values of $|A|$ for combinations of Z and ρ . The maximum scattering angle shown is $Z = 14$, which for the assumed value

of $X \sim 30$ is $\theta = 7/15$ rad, or about 27° . Larger angles (for this large an X) require a different type of series expansion of the integral than was used here.

However, the primary result of interest has already been obtained for this case: if $m - 1 \ll 1$, the intensity of the scattered light is not a function of θ and the scattered light retains the polarization of the incident beam.

Now, let us examine three extensions of this result in a qualitative way. Let the sphere become smaller. What happens to the scattering pattern?

In Figure 12, the scattering pattern will now change as long as $|m-1| \ll 1$, but will run to a greater terminal angle; that is, the pattern will expand to occupy a greater angular spread. For example, the part of the pattern shown will occupy the whole sphere when X is such that for $Z = 14$, $\theta = \pi$ rad. This will occur for $X = 14/\pi$, or $X = 4.5$. The particle radius (at 6300 Å) corresponding to this value of X is given by

$$a = \frac{X\lambda}{2\pi} = \frac{1}{2} \text{ microns.}$$

As the particle becomes so small that the upper left-hand region of the plot is alone applicable — that is, when $Z_{\max} \sim 2$ ($a \approx 1/15$ micron) and so $\rho = 0.45$ (with $n = 1.33$ for water) then the scattering is similar to Rayleigh scattering. If the treatment were exact, it should be Rayleigh scattering. However, in Rayleigh scattering it is well known that

$$s_1 = 1, \quad s_2 = k^3 a^3 \cos \theta \quad (9)$$

where α is the polarizability (isotropic case). Obviously, use of Equation 9 in Equations 2 and 3 will yield a polarization dependent

scattering intensity.

The treatment quoted for large particles is therefore scalar scattering, resulting from the assumption $m - 1 \ll 1$. The manner in which exact calculations (Mie theory) behave for values of X from 1 to 5, with $m = 1.33$, is shown in Figure 13. The solid curves are i_1 and the dotted curves are i_2 . That they will coincide eventually for sufficiently large X is not evident, and in fact for $m = 1.33$ will never occur. However, for large X the relative variations between i_1 and i_2 will become small and close together, and move toward small angles.

It is worth noting that $i_1 \approx i_2$ for $X = 2$, $m = 1.33$. This corresponds to water drops of $1/5$ micron radius; such drops will scatter light uniformly without regard to polarization of the incident beam, yet the scattered light will retain the polarization of the incident light. Such polarization independent scattering also will approximately occur for $X = 2.5$, $m = 1.55$ and for $X = 1.75$, $m = 1.50$. The index of refraction of polystyrene is 1.59 at 6300\AA . Thus, particles of $X = 2.5$ will have a scattering pattern essentially independent of θ , even for a polarized incident beam.

The conclusions for particles of $X < 30$, $m = 1.33$, are therefore that the scattering pattern is in general a function of θ for a polarized incident beam (except for certain selected values of X), and that the scattered light will retain the polarization of the incident beam.

In general: polarization of the scattered light from spherical, homogeneous, optically inactive substances of arbitrary size will be the same as that of the incident beam. Except for certain special values of X , or for $m - 1 \ll 1$ and X sufficiently large, the intensity of scattered light will depend upon θ , the angle of rotation of the scattered beam

from the incident beam polarization direction.

The reader is referred to Van de Hulst for details of calculations leading to these results.

Finally, in Figure 14 there is a plot of the scattered intensity as a function of radius of a water droplet, for the special angles $\theta = 0^\circ$ and $\theta = 180^\circ$. The penalty one pays for using backscattering is loss of intensity, and the penalty grows as the droplet grows.

I-1 The assumption $m-1 \ll 1$ enables one to neglect the contribution of the wave reflected from the surface of the droplet. Only the transmitted (refracted) and diffracted rays are considered.

I-2 "In the same plane as the incident light" means that the polarization of the scattered ray is identical to that of a ray reflected along the same path by a mirror placed in the incident beam (or by any sequence of mirrors).

APPENDIX II

Jack G. Dodd

The question of particle recoil from a focused incident laser beam has arisen. This problem is considered below.

The pressure exerted by light is given by

$$P = \frac{2S}{C}. \quad (1)$$

In the worst case of a reflecting surface (II-1), where S is the Poynting vector and C is the speed of light. This pressure, on the projected diametral area of a spherical particle of radius " a " will result in a force of

$$F = \pi a^2 P = \frac{2\pi a^2 S}{C}. \quad (2)$$

The acceleration of the particle will be

$$\ddot{r} = \frac{F}{M} = \frac{2\pi a^2 S}{\frac{4}{3}\pi a^3 \rho C} = \frac{3}{2} \frac{S}{a\rho C}. \quad (3)$$

This is an upper limit.

An argon laser may furnish as much as 10 watts, although not generally at a single wavelength. Assuming a good focus, a radius of 5 microns will be chosen for the focal spot. The focal area will then be

$\sim 7.5 \times 10^{-11} \text{ m}^2$. The Poynting vector

$$S = \frac{W}{7.5 \times 10^{-11}} \approx 10^{11} \text{ W/m}^2. \quad (4)$$

Assume $a = 10^{-6} \text{ m}$ (1 micron).

Let the scatterer be water, with $\rho = 10^3 \text{ Kg/m}^3$. Then

$$\ddot{r} \approx 5 \times 10^5 \text{ m/s}^2. \quad (5)$$

Assume the particle initially at rest. It will, under this acceleration,

attain a speed of 5×10^5 m/s in one second. Naturally it would move out of the focal area long before it attained any such speed. Since the distance it moves under constant acceleration

$$r = \frac{1}{2} \ddot{r} t^2, \quad (6)$$

the time required for the particle to move a distance equal to the diameter of the focal spot (10^{-5} m) will be

$$t = \sqrt{\frac{2 \times 10^{-5}}{5 \times 10^5}} = 10^{-5} \text{ sec},$$

at the end of which time it will be traveling

$$v = \ddot{r} t = 5 \text{ m/s}. \quad (7)$$

Actually, such a power density would certainly vaporize it. Only about 2.5×10^{-12} Kg-cal would be required; at the focal spot, about 10^{-3} Kg-cal/s would be incident on the particle. Absorption of only 10^{-4} of this would vaporize the drop in 10^{-5} second.

It would be wise to leave the beam unfocused. Otherwise, significant velocity errors might be generated.

(II-1). The cross-section for radiation pressure of a drop sufficiently larger than the wavelength of light has been shown by Van de Hulst to be about 20% of its geometric cross-section for the index of refraction $n = 1.33$. The geometric cross-section is assumed here.

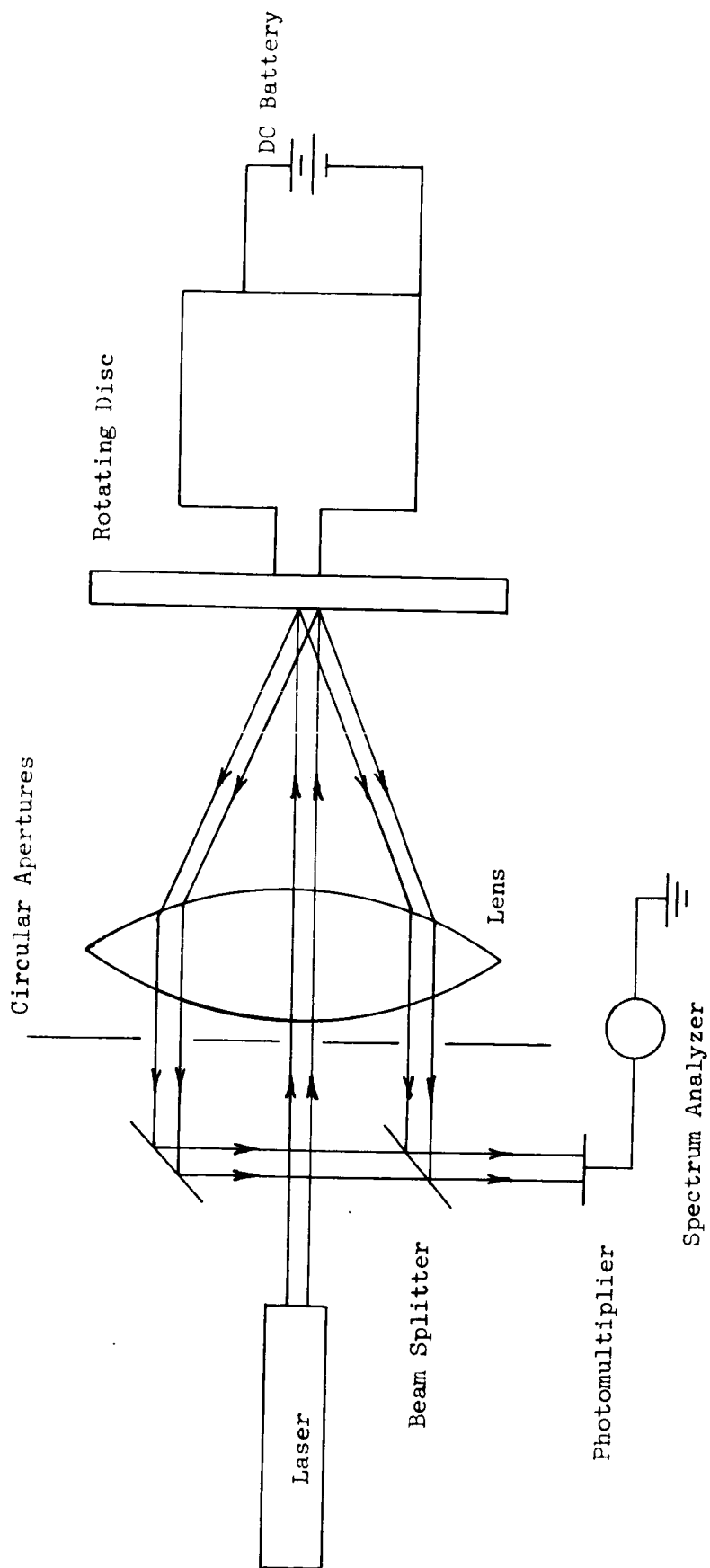


Figure 1

INITIAL EXPERIMENTAL ARRANGEMENT

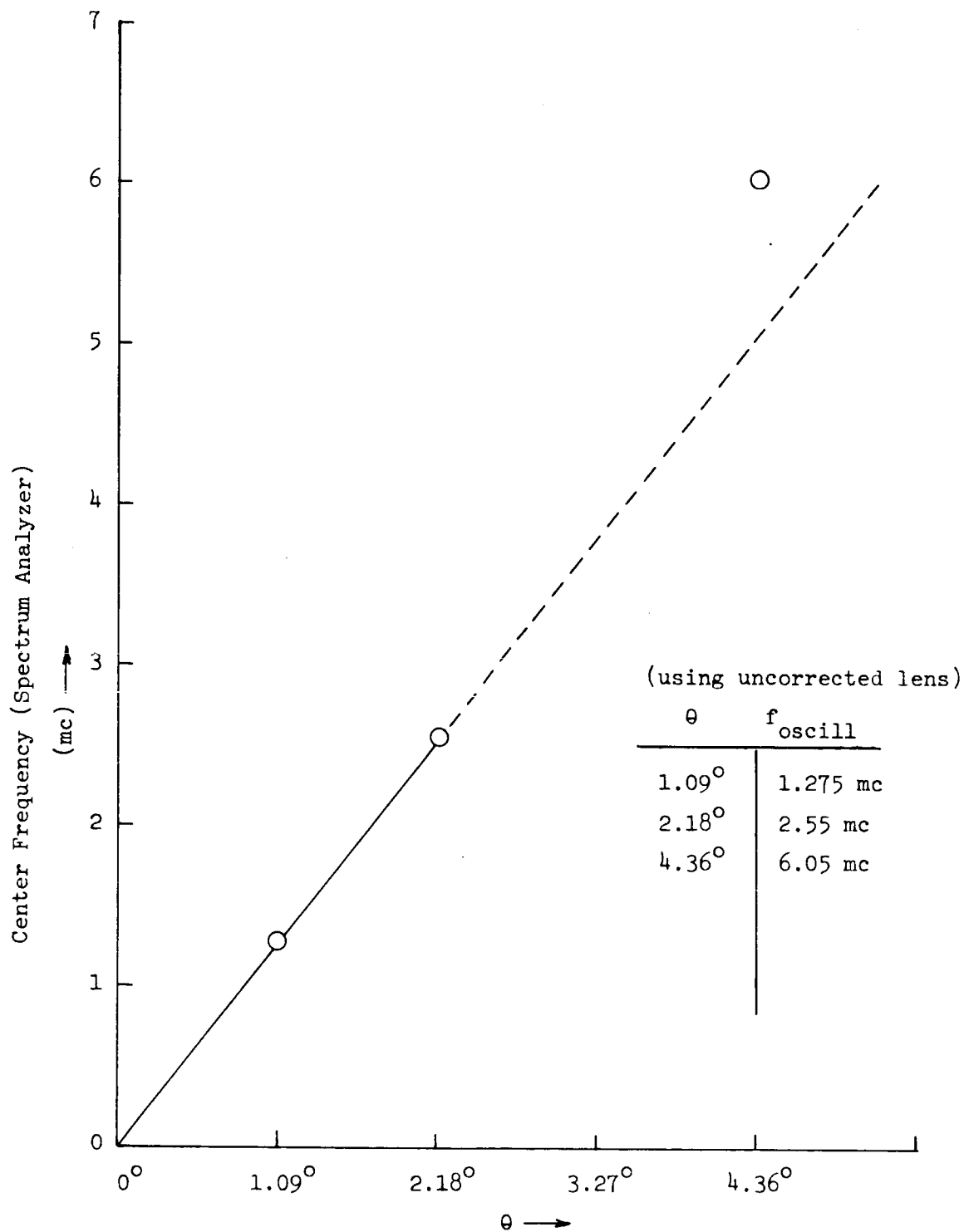


Figure 2

FREQUENCY READOUT ERROR FOR UNCORRECTED LENS

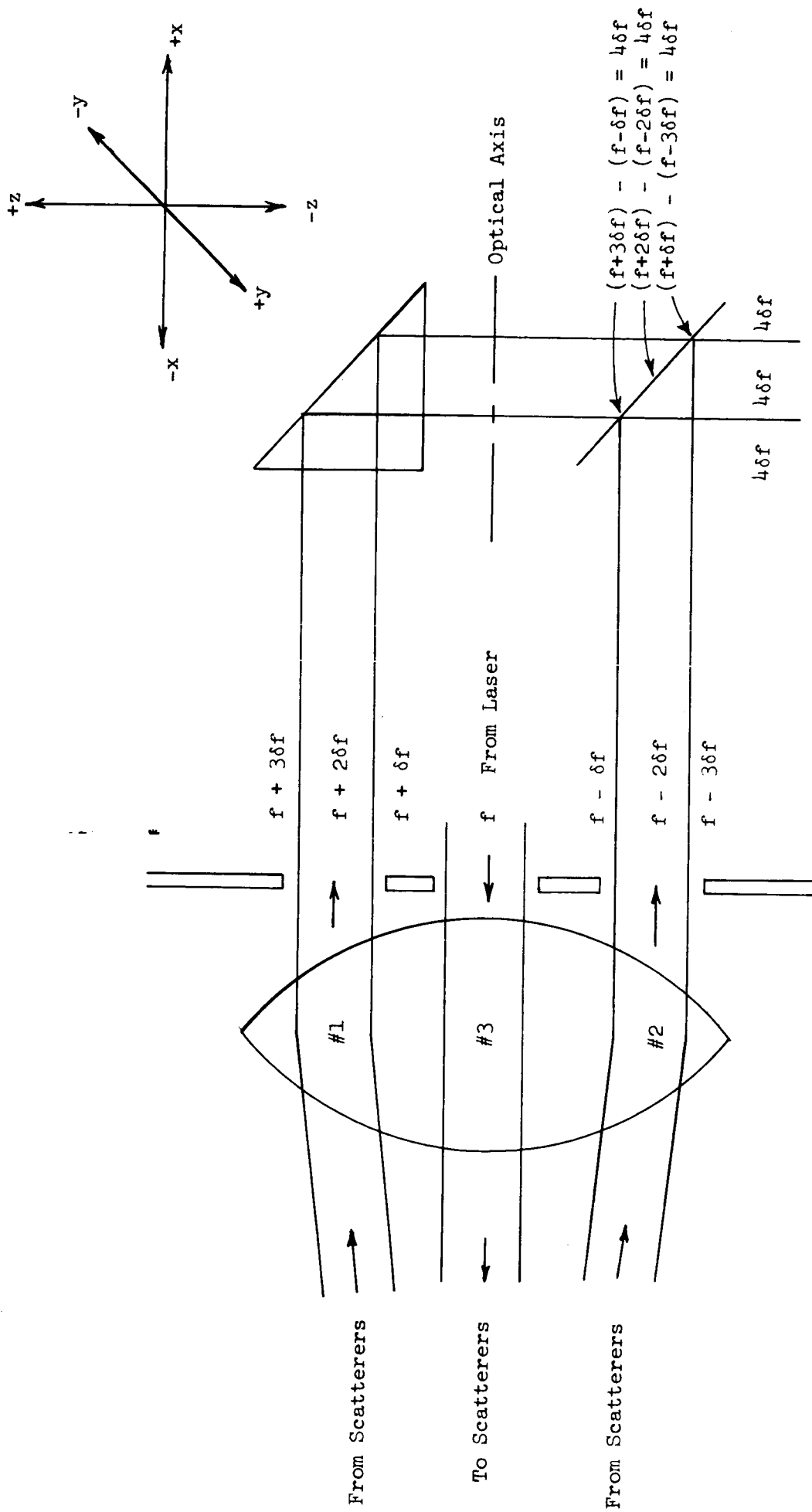


Figure 3
DETAIL OF MIXING ARRANGEMENT

$$\psi_1 = \psi + \frac{\theta}{2} = \psi_{\max}$$

$$\psi_2 = \psi - \frac{\theta}{2} = \psi_{\min}$$

$$\theta_1 = \theta + \frac{\theta}{2} = \theta_{\max}$$

$$\theta_2 = \theta - \frac{\theta}{2} = \theta_{\min}$$

$$\frac{\theta}{2} = 10 \text{ min}$$

$$\theta = 6^\circ$$

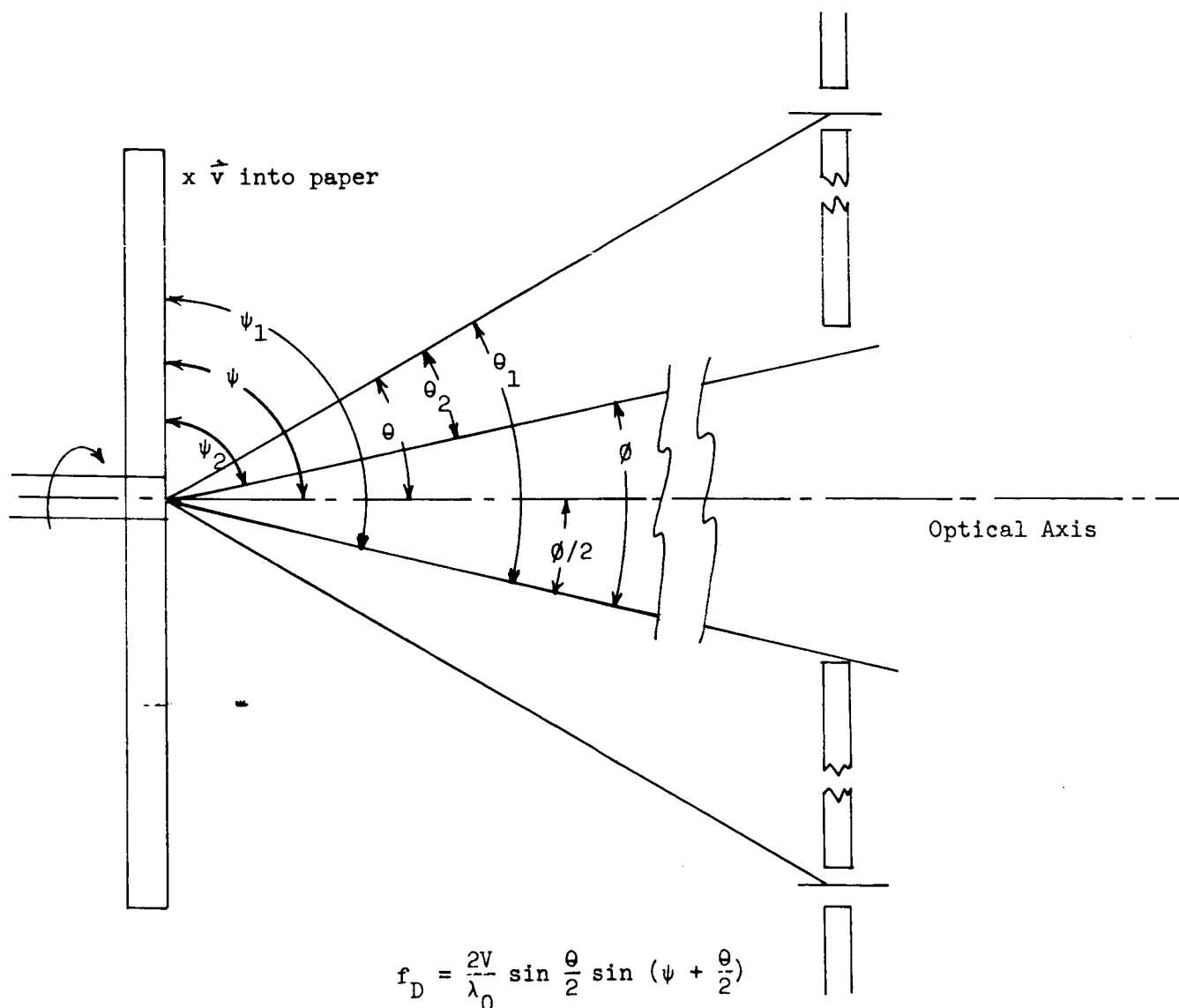
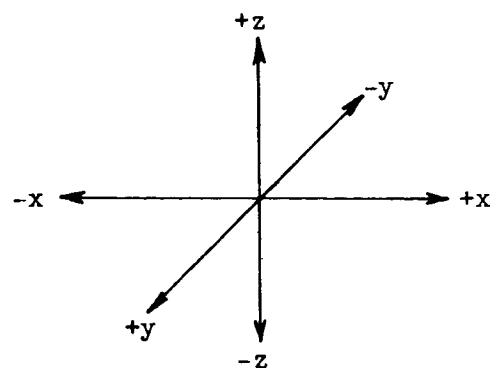


Figure 4

EFFECT OF BEAM CONVERGENCE ON FREQUENCY SPREAD

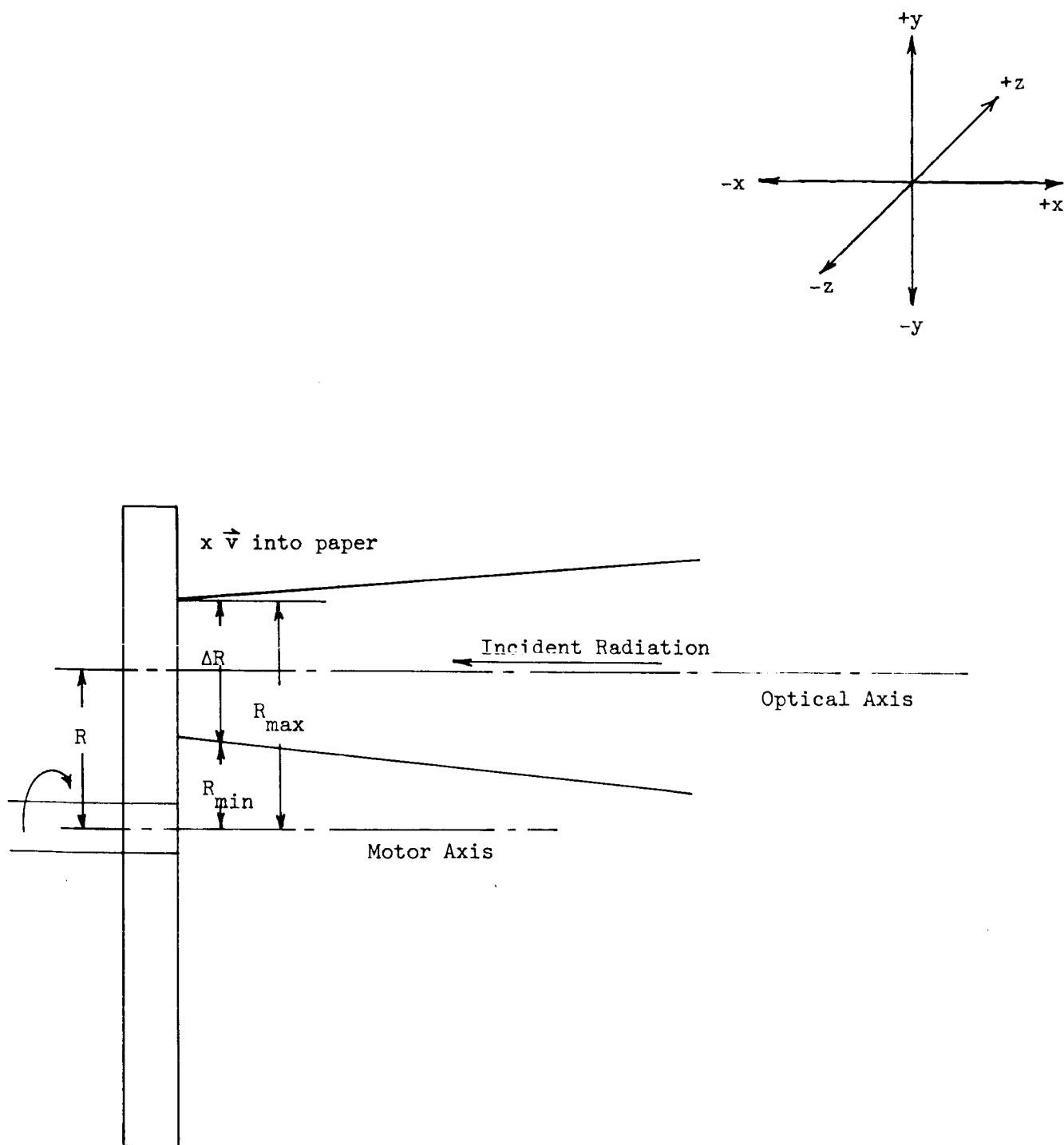


Figure 5

EFFECT OF VERTICAL DIMENSION OF FOCUSED SPOT ON FREQUENCY

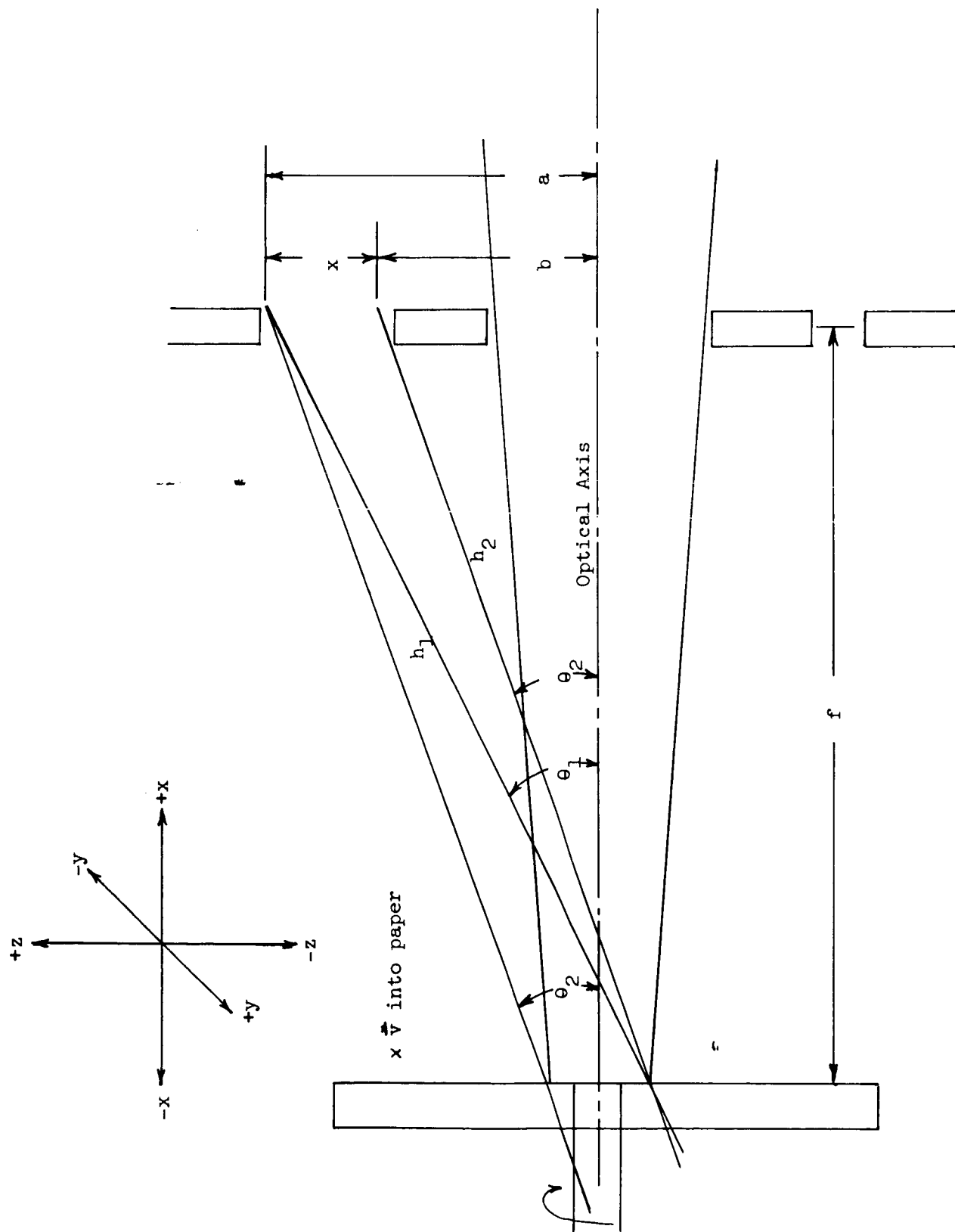


Figure 6
CONTRIBUTION OF HORIZONTAL BEAM SIZE TO FREQUENCY SPREAD

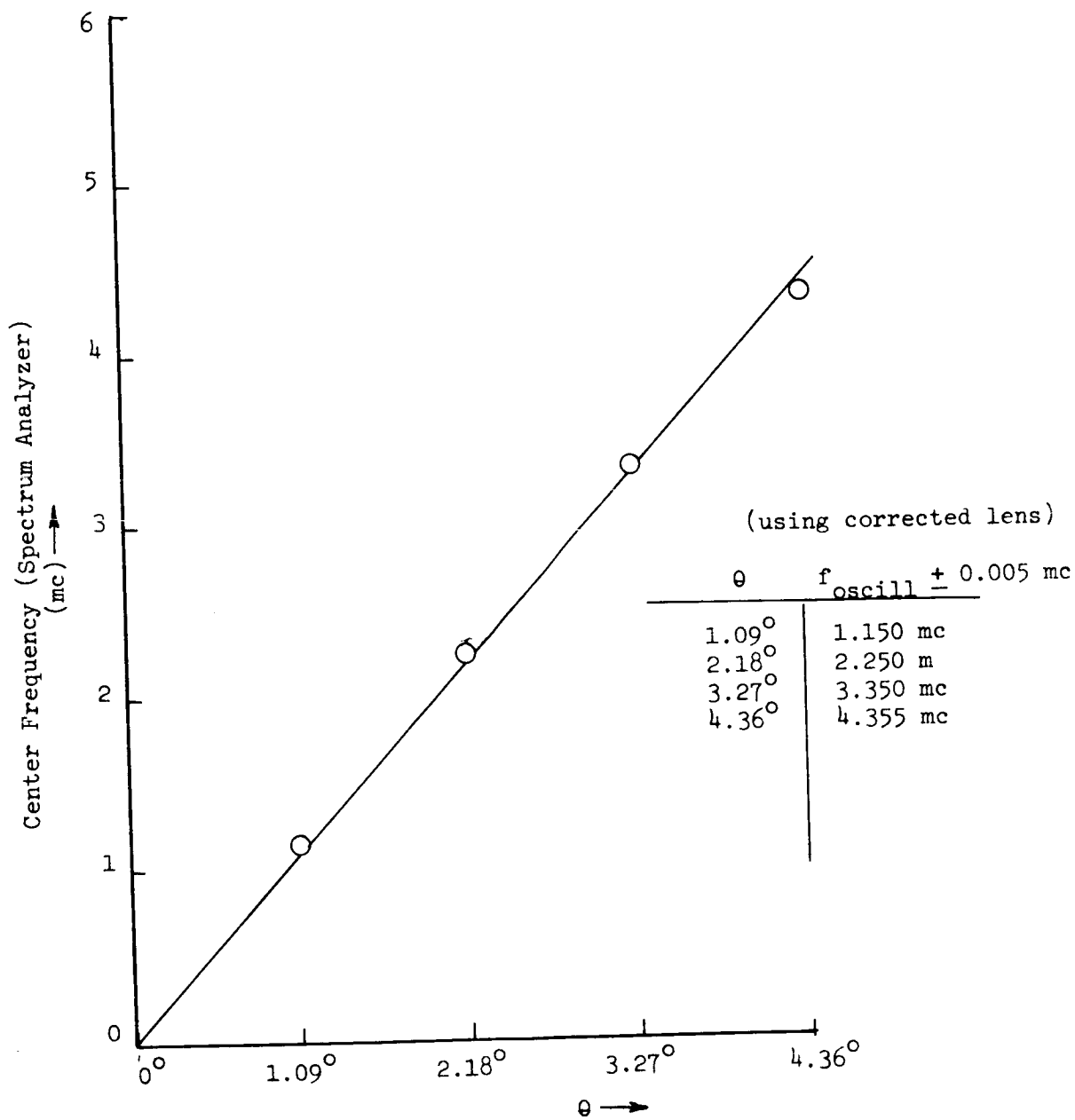


Figure 7
FREQUENCY READOUT ERROR FOR CORRECTED LENS

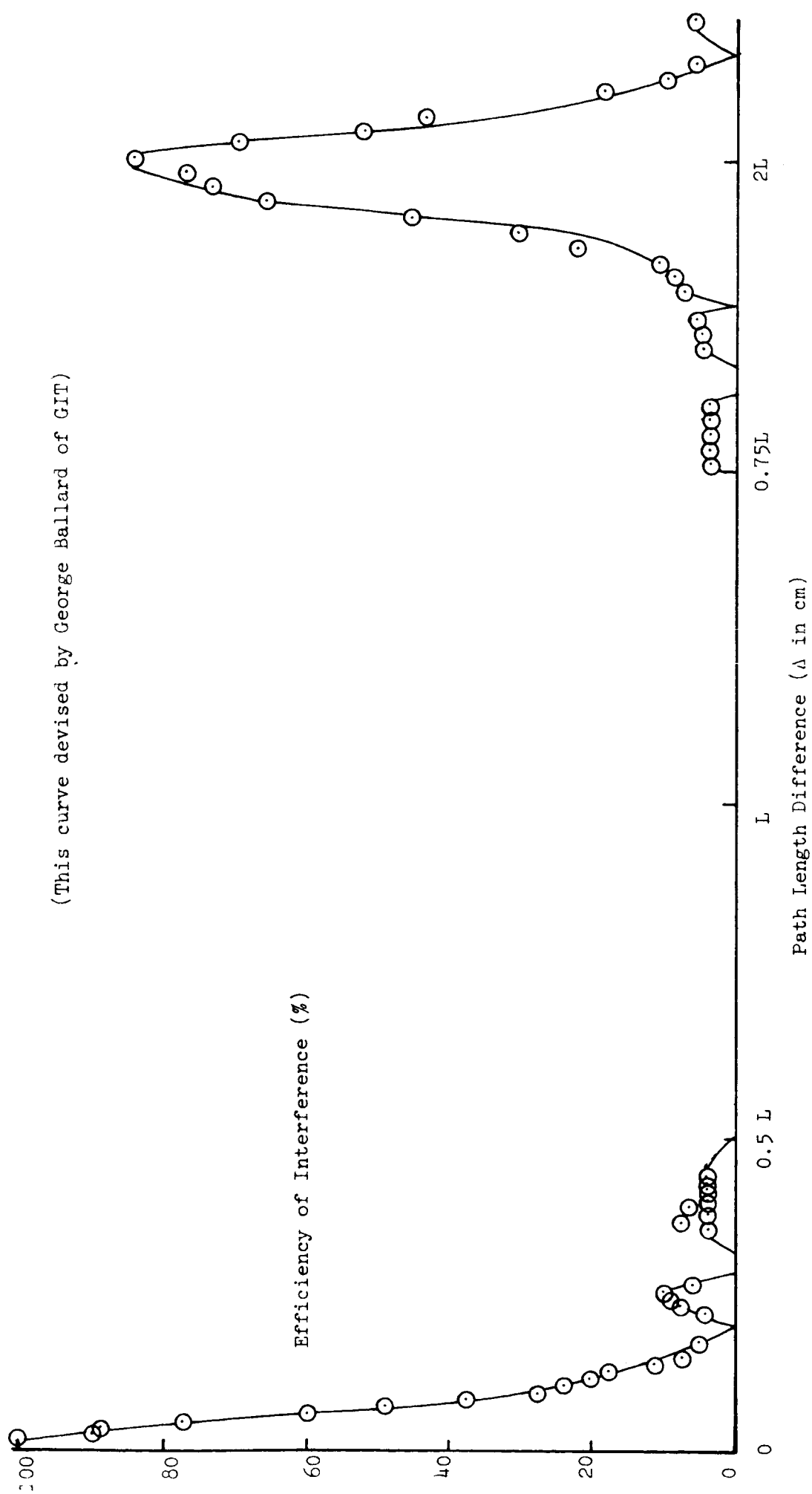


Figure 8

LONGITUDINAL MODE EFFECTS OF SPECTRA PHYSICS MODEL 125. (CAVITY LENGTH $L = 180$ cm)

A = Dielectric Mirror
 B = Lens
 C = Dielect Mirror
 D = Optical Path Length Compensator
 E = Cube Beam Splitter

F = Gold Mirror to Reflect Second
 Heterodyned Signal Onto Photocathode
 G = Photocathode
 H = Photomultiplier
 I = Spectra Physics Model 125 Laser (74mW Output)
 J = Synchronous Motor
 K = Frequency Generator (300-500 cps, 120 V)

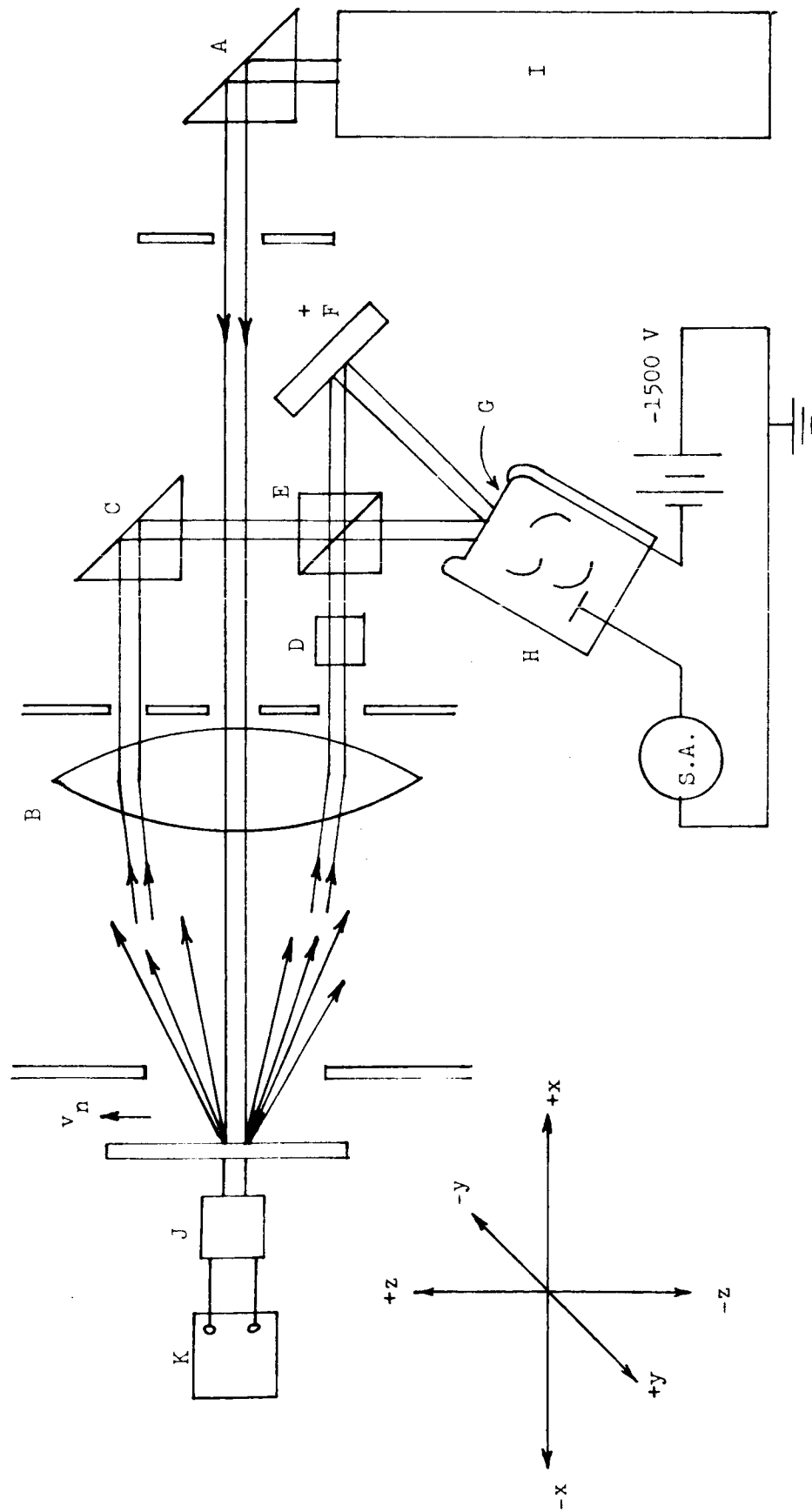


Figure 9
 CURRENT EXPERIMENTAL ARRANGEMENT

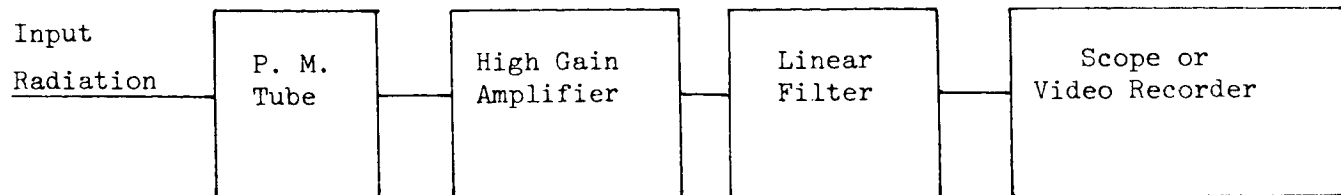


Figure 10
CIRCUIT DIAGRAM

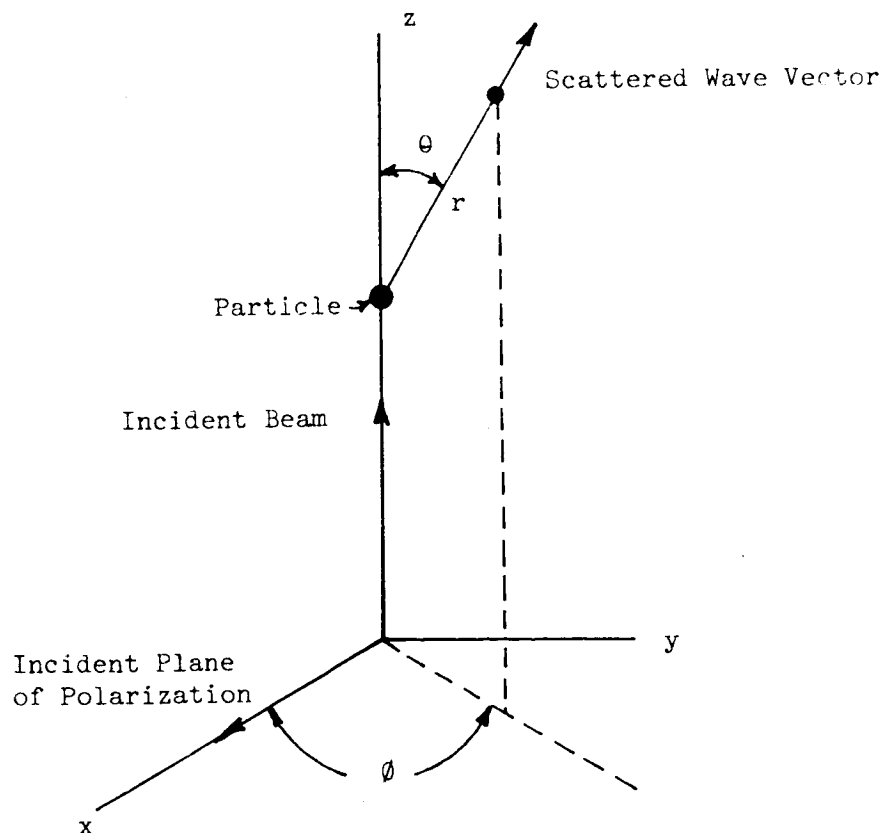


Figure 11
SCATTERING DIAGRAM

VALUES OF THE AMPLITUDE FUNCTION

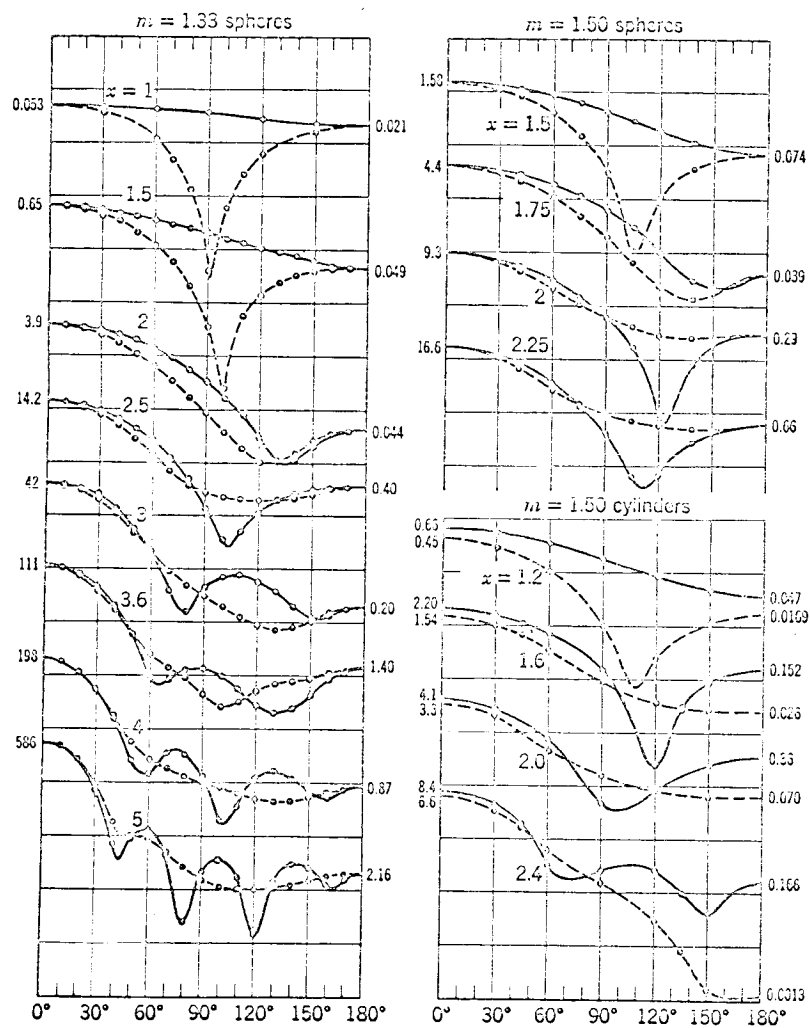


Figure 13

SCATTERING INTENSITY PLOTS

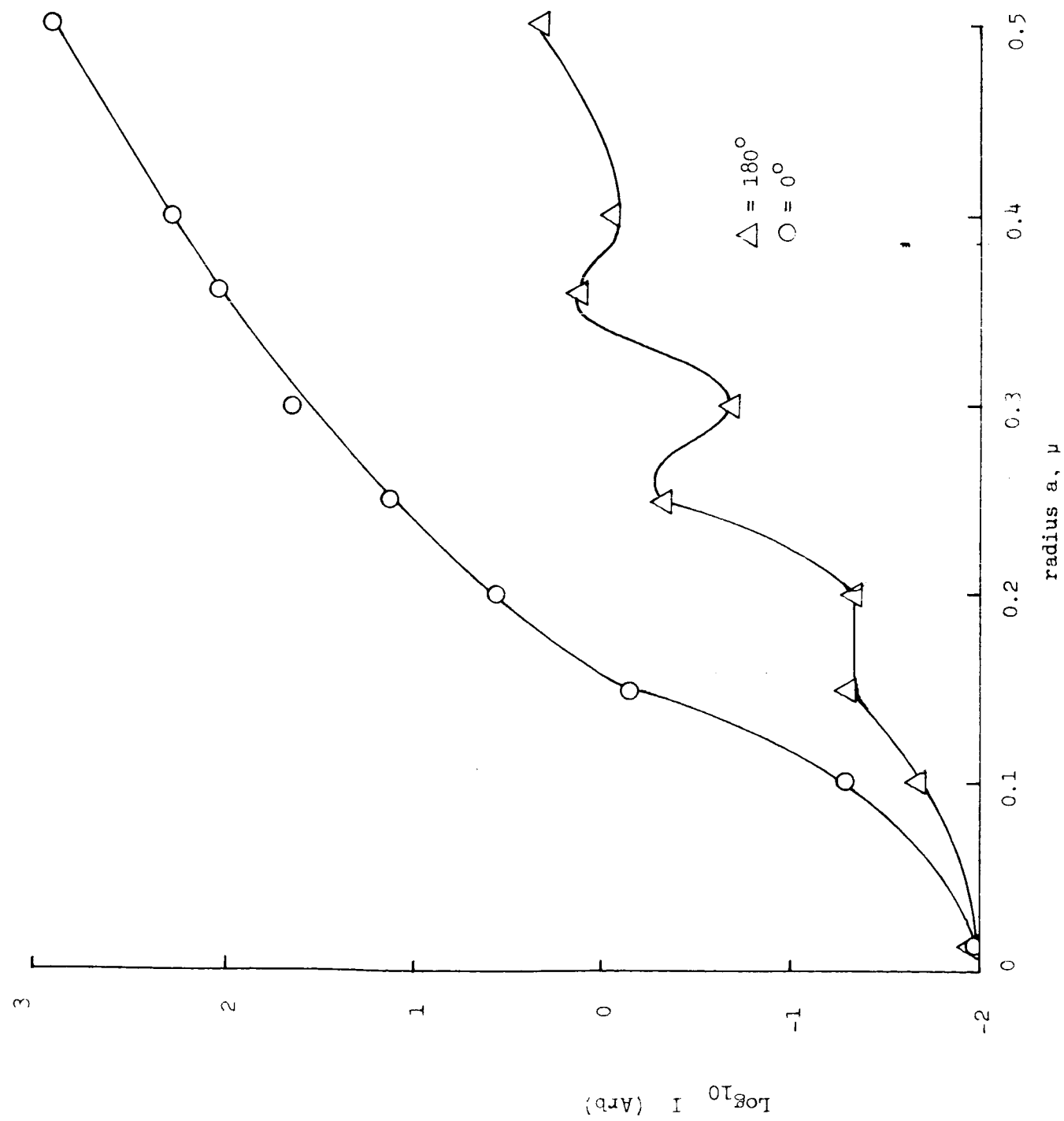


Figure 14

SCATTERED INTENSITY AT 0° AND 180° AS A FUNCTION OF DROPLET RADIUS, FOR WATER. $\lambda = 6328\text{\AA}$